AGU ADVANCING EARTH AND SPACE SCIENCES

JGR Atmospheres

RESEARCH ARTICLE

10.1029/2024JD043253

Evaluation of Satellite-Based Lightning NO_x Columns Using In-Cloud Aircraft Measurements

Madilynn Seiler[1], Kenneth Pickering[1], Dale Allen[1], Eric Bucsela[2], and Heidi Huntrieser[3]

[1]Department of Atmospheric and Oceanic Science, University of Maryland, College Park, MD, USA, [2]Science, Systems, and Applications, Inc., Lanham, MD, USA, [3]Institut für Physik der Atmosphäre, Deutsches Zentrum für Luft- und Raumfahrt (DLR), Oberpfaffenhofen, Germany

Key Points:

- Differences between satellite-retrieved and aircraft-retrieved lightning-NO_x columns range from ~20% to ~50%
- Uncertainty estimates for satellite-based LNO_x columns would benefit from additional in-cloud aircraft NO_x profiles
- LNO_x production efficiencies, using ozone monitoring instrument retrievals for three case studies, range from 52 to 691 mol/flash

Supporting Information:

Supporting Information may be found in the online version of this article.

Correspondence to:

M. Seiler,
mseiler1@umd.edu

Citation:

Seiler, M., Pickering, K., Allen, D., Bucsela, E., & Huntrieser, H. (2025). Evaluation of satellite-based lightning NO_x columns using in-cloud aircraft measurements. *Journal of Geophysical Research: Atmospheres*, *130*, e2024JD043253. https://doi.org/10.1029/2024JD043253

Received 23 DEC 2024
Accepted 17 AUG 2025

Abstract

Lightning is the largest source of NO_x in the upper troposphere, where it affects the distributions of tropospheric ozone, hydroxyl radical (OH), and methane. In this study, ozone monitoring instrument (OMI)-based LNO_x columns are evaluated using aircraft-based columns from case studies during the Deep Convective Clouds and Chemistry (DC3), the Tropical Composition, Cloud, and Climate Coupling (TC^4), and African Monsoon Multidisciplinary Analysis (AMMA) campaigns. This is the first time OMI LNO_x column amounts have been evaluated using in situ data from aircraft profiles. For each case study, aircraft transects of the storm anvils were completed near the time of the OMI satellite overpass, allowing for direct comparison of satellite-retrieved and aircraft-sampled LNO_x columns from the cloud top to the OMI optical centroid pressure. These comparisons were used to assess uncertainties in the satellite-based columns. Differences between the aircraft and mean OMI LNO_x column amounts varied with location and flash density. The DC3 and TC^4 cases resulted in OMI column amounts 38%–56% less than the aircraft, while for the AMMA case, the OMI column was 20%–30% larger than the aircraft column. These differences are consistent but slightly larger than the 36% uncertainty estimated for the satellite retrieval method. Additionally, mean LNO_x production efficiency (PE) was determined with values ranging from 52 to 691 mol/flash. These findings lend support for on-going LNO_x PE estimates using OMI, TROPOMI, TEMPO, GEMS, and Sentinel-4 data and show the need for additional aircraft profiles to further reduce uncertainties.

Plain Language Summary

Lightning is a major source of nitrogen oxides (NO_x) in the upper atmosphere, where it influences key chemical constituents that affect climate and air quality. This study compares satellite measurements of lightning-produced NO_x columns from the ozone monitoring instrument satellite instrument with columns derived from aircraft measurements collected during three field campaigns that occurred over the central United States, tropical ocean near Costa Rica, and tropical land in Western Africa. Aircraft flew within thunderstorms close to the time the satellite passed overhead, allowing for a direct comparison. The results show that satellite-derived columns were sometimes lower or higher than aircraft observations, depending on the region and lightning activity. Overall, the differences were close to the expected uncertainty for the satellite data. The study also estimates how much NO_x is produced by each lightning flash. These results support continued use of satellite observations to study lightning impacts and show that more aircraft data are needed to improve accuracy.

1. Introduction

Formation of NO by lightning occurs when O_2 and N_2 bonds dissociate in the extreme heat of the flash channel. When the channel cools, O and N atoms form NO (Zeldovich et al., 1947). NO then rapidly reacts with O_3, and equilibrium is quickly reached between NO and NO_2. The resulting sum of NO and NO_2 is designated as NO_x. The production of NO_x due to lightning (LNO_x) has been a long-studied topic of atmospheric chemistry due to its effects on the upper tropospheric (UT) composition and production of ozone. Along with ozone, OH is enhanced due to LNO_x production and subsequently affects the methane budget (Labrador et al., 2004). According to DeCaria et al. (2005) and Pickering et al. (2024), approximately 10 ppbv of ozone is produced downwind of midlatitude convective storms during the 24-hr period following a convective system. Recently, Pickering et al. (2024) estimated a mean NO_x production by lightning of 80–110 mol per flash in a very high flash rate storm. Pickering also investigated the downwind production of ozone following convection and found that photochemical ozone production in LNO_x enhanced areas occurred at a rate of 10–11 ppbv per day in the upper troposphere. Despite its significant contribution to atmospheric chemistry, the amount of NO_x produced per flash and globally still contains considerable uncertainty.

According to Schumann and Huntrieser (2007), the annual global LNO_x emission has the range 5 ± 3 Tg. Lightning is the source of 80% of the free troposphere NO_x production in the UT subtropics, tropics, and summer midlatitudes (B. Nault et al., 2017). Subsequently, the production of NO_x in the UT accounts for up to 55% of UT ozone production in the tropics and 35% in the summertime in the United States (D. Allen et al., 2012). An increase in LNO_x production per flash by a factor of four could lead to a 60% increase in the tropospheric ozone (Liaskos et al., 2015). Anthropogenic emissions of NO_x have been decreasing rapidly due to the implementation of the Clean Air Act and other EPA regulations in the United States. In China, NO_x emissions have decreased up to 20% in some areas (Jamali et al., 2020; Liu et al., 2017). Europe experienced a 46% decrease in NO_x from 2000 to 2017 (Sicard et al., 2021). Decreases in NO_x make lightning an increasingly important source (Q. Zhu et al., 2019). Future changes in the lightning source of NO_x are uncertain as global warming could lead to an increase or decrease in the frequency of lightning strikes (D. L. Finney et al., 2018; Romps et al., 2014).

LNO_x production has been quantified using satellite observations of NO_2 coupled with lightning data. Beirle et al. (2006) used GOME NO_2 total column density measurements over the Gulf of Mexico to predict a production efficiency (PE) average of 90 mol/flash with NLDN measured flashes. The range from this study was 32–240 mol/flash. Beirle et al. (2010) used data from SCIAMACHY along with World Wide Lightning Location Network (WWLLN) lightning and found very little LNO_x signal for high flash rate storms. Bucsela et al. (2010) were the first to apply ozone monitoring instrument (OMI) NO_2 columns in estimating LNO_x production. Bucsela's study used OMI pixels over clouds and over nearby outflow during the TC^4 campaign based in Costa Rica. Pickering et al. (2016) instead focused on the OMI deep convective pixels over the Gulf of Mexico and obtained mean LNO_x production of 80 mol/flash. OMI NO_2 column amounts were used in D. J. Allen et al. (2019) to find tropical lightning produced 170 ± 100 mol/flash with largest values over the tropical Pacific. This study used linear regression between flashes and OMI LNO_x to estimate PE, in both continental and marine locations, where previously PE was often computed using a summation approach (Bucsela et al., 2010; Pickering et al., 2016). It was found that lightning in tropical marine locations produces approximately two times as much NO_x per flash as flashes in tropical continental regions. Bucsela et al. (2019) used OMI in LNO_x studies over the midlatitude continents and found that there is an inverse relationship between flash rate and PE. Using the Tropospheric Monitoring Instrument (TROPOMI), D. J. Allen et al. (2021) obtained a PE of 175 ± 100 mol/flash using Geostationary Lightning Mapper data. In Allen's analysis, there was a positive relationship between flash energy and the production of LNO_x. Using the TROPOMI satellite and the Erbo Lightning Mapping Array, Pérez-Invernón et al. (2023) found a PE of 58 ± 44 mol/flash of NO_x using one method to remove the background and 108 ± 82 mol/flash using an alternative method. This study emphasized that the positive relationship between the channel length and LNO_x per flash is sensitive to the vertical structure of the lightning flash and how the branches of the flash are distributed at different altitudes. Using two new sets of OMI cloud-sliced observations created by NASA and the Royal Netherlands Meteorological Institute, Marais et al. (2018) were able to address uncertainties in NO_x sources in the UT. Aircraft observations from numerous campaigns were compared to OMI NO_2 retrievals. Further insight on UT NO_x from lightning emissions were observed through GEOS-Chem CTM simulations. Through these simulations, it was concluded there were no major differences in NO_x production efficiencies between midlatitudes and tropics. Marais et al. (2018) derived a global mean PE of 280 ± 80 mol/flash.

Estimates of LNO_x production rates per flash based on aircraft data range from 16 to 700 mol NO_x/flash (Bucsela et al., 2010; DeCaria et al., 2005; Ott et al., 2010; Schumann & Huntrieser, 2007; Q. Zhu et al., 2019). These wide differences were obtained from several field campaigns including TROCCINOX in southern Brazil (Huntrieser et al., 2007, 2008), SCOUT-O3 in Australia (Huntrieser et al., 2009), AMMA in West Africa (Huntrieser et al., 2011), and the DC3 in the Central United States (I. Pollack et al., 2016). During the 2005 TROCCINOX campaign, average NO_x enhancements due to lightning ranged from 0.2 to 1.2 ppbv. Differences in LNO_x production between tropical and subtropical storms were attributed to differences in vertical wind shear causing differences in stroke lengths within the storms. In the DC3 campaign, I. Pollack et al. (2016) quantified LNO_x production over the Great Plains and obtained a PE range of 142–291 mol/flash for the three best sampled storms. The field campaign, SCOUT-O3, in 2005 analyzed thunderstorms over northern Australia. A given range for intense tropical island convection was 292–342 mol of NO_x per flash.

Modeling LNO_x is difficult as uncertainties in flash rate and LNO_x production per flash are large. Flash rate schemes in global and regional models include Price and Rind (1992), dependent heavily upon cloud top height, and D. Finney et al. (2014), which is based on the vertical ice-mass flux. A more recent approach was made by Stolz et al. (2017), who parameterized lightning using multiple variables such a cloud condensation nuclei, warm cloud depth, and normalized CAPE. Uncertainty in modeling estimation also lies in the amount of LNO_x produced in each type of flash, that is, cloud-to-ground (CG) or intracloud (IC). Modeling by Koshak et al. (2014) found that cloud-to-ground (CG) flashes produce more LNO_x per flash than intracloud (IC) flashes. A similar conclusion was reached by Lapierre et al. (2020), who also reported that CG flashes generate more NO_x than IC flashes. However, other studies involving cloud-resolving modeling constrained by observed flash rates and aircraft anvil NO_x observations show that on average there is very little difference between the two types (Cummings & Cummings, 2013; DeCaria et al., 2005; Ott et al., 2010; Pickering et al., 2024). The CMAQ model approach taken by D. Allen et al. (2012) parameterized flash frequency in terms of convective precipitation and specified emissions of lightning under the parameters of flash frequency, flash energy, and NO production per unit energy. The inclusion of LNO_x production reduced mean biases in nitrate wet deposition to near zero. Using the GMI model, D. Allen et al. (2010) tested multiple simulations with varying amounts of lightning NO emissions using aircraft and satellite data. This approach estimated that, globally, 60%–70% of UT NO_x and 35%–45% of UT ozone has a lightning source concluding that lightning plays a very large role in UT chemistry. Martin et al. (2007) used a global chemical transport model (GEOS-Chem) to identify locations of lightning events and then investigated those areas using observations from multiple satellites including SCIAMACHY and OMI. They found that a global source of 6 ± 2 Tg N yr^{-1} best represents the satellite-retrieved NO_2 and O_3 columns.

The main sinks of NO_x in the UT near-field convective outflow are the reactions forming alkyl and peroxy nitrates. An important uncertainty to address is the rate at which these reactions take place, that is, the lifetime of NO_x in the near field of convection. It was concluded by B. A. Nault et al. (2016) that the decay of NO_x is consistent with the formation of secondary oxidized nitrogen species and dependent on volatile organic compound (VOC) concentrations. This uncertainty is addressed further in Section 5.

Our current study is in part an evaluation of the technique described in Bucsela et al. (2019) for calculating LNO_x from OMI. Bucsela et al. (2019) combined satellite observations with ground-based lightning flash counts to obtain a mean PE of 180 ± 100 mol per flash for midlatitude continental regions. This value was obtained by converting OMI slant column densities (SCDs) of NO_2 to vertical column densities of LNO_x by using an air mass factor (AMF) based on LNO_x and LNO_2 profiles from a chemical-transport model. The technique used in estimating vertical column amounts of LNO_x is further detailed in Section 2.1. The present study examines the validity of this technique by comparing OMI column amounts to those computed from in situ aircraft observations in three different case studies. All previous satellite-based LNO_x analyses have been performed without benefit of comparisons with in situ aircraft measurements. The DC3, TC^4, and AMMA campaigns provide observations that can be used to evaluate the OMI-based estimates and their uncertainty.

2. Data

2.1. OMI

The OMI instrument aboard the Aura satellite, which launched in 2004, is an ultraviolet-visible spectrometer that is sun-synchronous and crosses over the equator at 13:45 LT daily. The instrument measures radiances with a linear array of sensors in a continuous swath (Levelt et al., 2006). These radiances can then be used to retrieve SCDs of NO_2. The OMI satellite instrument provides data from pixels that are, at minimum, 13×24 km. The orbital swath, the strip of earth covered by the satellite's sensors, is 2,600 km per orbit with nearly 15 orbits each day. The retrievals are performed by the OMI team (Lamsal et al., 2021) at NASA Goddard Space Flight Center. The Version 4.0 products provide total, tropospheric, and stratospheric NO_2 VCDs retrieved from radiance and irradiance data from the visible channel. Products produced by the OMI also include SCD of NO_2, and tropospheric and stratospheric AMFs. General details on AMF calculations can be found in Palmer et al. (2001). Improvements to the OMI retrievals implemented in Version 4.0 are listed in detail in Lamsal et al. (2021), which include a new spectral fitting algorithm for the operational NO_2 product (Marchenko et al., 2015) using a differential optical absorption spectroscopy approach. Improvements in the tropospheric AMF are also included in the new product. Of note, in 2007, the OMI instrument experienced a defect known as the row anomaly described in Schenkeveld et al. (2017) where the blockage effect, solar light contamination, wavelength shift, and earth

Table 1
Instrumentation Used on 11 June DC3 Campaign, 5 August TC^4 Campaign, and 6 August African Monsoon Multidisciplinary Analysis Campaign

Case	Aircraft	Species	Method	Uncertainty	Reference
11 June	DC-8	NO, NO_2	Chemiluminescence, TDLIF	±4%, ±10%	Ryerson et al. (2000), Thornton et al. (2000)
		CO	Diode Laser Spectrometer	±2%	Sachse et al. (1991)
		VOC	Whole Air Sampler	Species dependent	
	GV	NO, NO_2	Chemiluminescence, UV Photolysis	±10%, ±15%	Ridley and Grahek (1990)
		CO	Vacuum UV Fluorescence	±3%	Gerbig et al. (1999)
	Falcon	NO_x	UV Photolysis	±30%	I. B. Pollack et al. (2010)
		CO	Vacuum UV Fluorescence	±5%	Gerbig et al. (1999)
5 August	DC-8	NO, NO_2	Chemiluminescence, TDLIF	±4%, ±10%	Ryerson et al. (2000), Thornton et al. (2000)
		CO	Diode Laser Spectrometer	±2%	Sachse et al. (1991)
6 August	Falcon	NO, NO_x	Chemiluminescence, calculated via photostationary state	±1 pmol/mol	Volz-Thomas et al. (1996)
		CO	Vacuum UV Fluorescence	10%	Gerbig et al. (1996)
11 June	DC-8	Cloud	Video Footage	–	
	GV	Cloud	2D-s Probe	–	Lawson et al. (2006)
	Falcon	Cloud	Forward Scattering Spectrometer Probe	–	
5 August	DC-8	Cloud	2D-s Probe	–	Lawson et al. (2006)
6 August	Falcon	Cloud	Forward Scattering Spectrometer Probe	–	

Note. Uncertainties listed in I. Pollack et al. (2016) and Huntrieser et al. (2011).

radiance have all negatively affected some of the OMI pixels (defined as rows 25–42). In this study, the OMI row anomaly hindered the ability to retrieve NO_2 in the 11 June 2012 case (see Section 4.1.2). This study utilizes data from the OMI instrument rather than TROPOMI, as the case studies analyzed took place prior to TROPOMI's launch in 2017. Moreover, no comparable field campaigns focused on the atmospheric composition within deep convection or near-field outflow have been conducted since TROPOMI became operational.

2.2. Aircraft Data

In situ data for each case study were reported at a temporal resolution of 1 s and were obtained from the NASA DC-8, NSF/NCAR GV, and/or the DLR Falcon depending upon the case. Instrumentation for each plane is given in Table 1. The campaigns chosen are such that there are valid aircraft measurements aligned nearly temporally and spatially with the OMI overpass. Vertical profiles for all three case studies show a large enhancement of NO_x in the altitude range of 9–13.5 km indicating that lightning was prevalent in all cases. All species measured are taken at a variety of altitudes in or near the anvil of the storm.

2.3. Lightning Data

Lightning data are necessary for the determination of LNO_x PE. Lightning data sets used for the three case studies are described as follows:

2.3.1. ENTLN

The Earth Networks Total Lightning Network (ENTLN) is a lightning locating system which detects low-frequency sferics within the range of 1 Hz-12 MHz for cloud-to-ground and intracloud flashes (Marchand et al., 2019). Included in the ENTLN data set are flash characteristics such as time, latitude, longitude, type, peak current, polarity, and multiplicity. Through the evaluation done by Y. Zhu et al. (2017) on ENTLN detection efficiency (DE) DE, the current ability of the network is 100% DE on CG flashes and 90% DE on IC flashes (Quick et al., 2017). At the time of analysis for the 11 June 2012 case study, the DE of ENTLN was 100% for CG and 60% for IC.

2.3.2. WWLLN

The World Wide Lightning Location Network (WWLLN) is a large network of very low-frequency radio sensors operated by the University of Washington. The network employs the TOGA (time of group arrival) method to pinpoint lightning strokes by analyzing sferic waveforms at each WWLLN station (Dowden et al., 2002; E. H. Lay et al., 2004; E. Lay et al., 2005). The detection range for WWLLN is 3–30 kHz and the network is most efficient at detecting high-energy CG strokes (Rodger et al., 2009). As of April 2006, there were 25 stations providing coverage (Rodger et al., 2006). Since then, the expanse of the network has increased greatly; however, two of these case studies for this analysis occurred in 2006 and 2007. The DE used in these cases is case-dependent and is described in further detail in the sections below.

3. Methods

3.1. OMI Analysis

In the Bucsela et al. (2019) analysis, the SCDs of NO_2 are converted to vertical columns of LNO_x^* (vertical column amounts of NO_x over deep convection before subtraction of background NO_x due to sources other than recent lightning, such as nonrecent lightning or boundary layer pollution). We consider pixels with an optical centroid pressure (OCP) of less than 500 hPa and a cloud radiative fraction greater than 0.95 for the 11 June case and 0.90 for the 5 and 6 August case. These pixels are deemed "deep convective" pixels. The cloud threshold for each case is chosen as a compromise between the need to have sufficient pixels and the desire to minimize the contribution from the planetary boundary layer (PBL). Stratospheric contributions to the initial column amounts are removed by a zonal stratospheric smoothing method that eliminates any longitudinal variation in the tropopause height which could falsely assign some LNO_x to the stratosphere $V_{\text{stratZonal}}$. The full equation used by Bucsela et al. (2019) is given as Equation 1.

$$LNO_x^* = (S - V_{\text{stratZonal}} A_{\text{strat}}) / A_{LNOx} \quad (1)$$

The OMI total SCD of NO_2 is given as S. The zonally averaged stratospheric vertical column density is given as $V_{\text{stratZonal}}$. The $V_{\text{stratZonal}}$ variable is multiplied by the stratospheric AMF, A_{strat}, to obtain the stratospheric SCD. The AMF relates the NO_2 concentration along the mean photon path through the atmosphere before reaching the satellite to the vertical column amount above the pixel being measured. The stratospheric AMF is dependent on viewing geometry and is a product of the OMI retrieval algorithm. Uncertainty in the calculation of the tropospheric AMF is one of the largest sources for error in NO_2 retrieval (Lorente et al., 2017). In Equation 1, A_{LNOx} represents the AMF that converts the tropospheric NO_2 slant column to the NO_x vertical column. For this analysis, the AMF is computed using profiles of NO_2 and NO_x from cloud-resolved model simulations of thunderstorms by Ott et al. (2010). The OMI-based estimate of the LNO_x column is sensitive to a priori vertical distribution of LNO_x as retrieval sensitivity varies with height. The profile of LNO_x is assumed to match those simulated in Ott et al. (2010) through a three-dimensional cloud-scale chemical transport model with parameterized sources of lightning NO_x.

The LNO_x^* over deep convective pixels is multiplied by the pixel area and summed over $1° \times 1°$ grid cells and provided for the current study as a gridded data set of $1° \times 1°$ grid cells of moles of LNO_x^*, which for comparison with aircraft data were converted to molecules per cm^2. With OMI pixel sizes ranging from 13×24 km to greater than 100 km, it was necessary to use $1° \times 1°$ degree grid cells to obtain a representative sample in each cell. Two methods were used to remove background NO_x and obtain the vertical column of lightning-produced NO_x. The approach taken in Bucsela et al. (2019) attributed 15% of the column to background sources. This value was based on modeling studies by DeCaria et al. (2000), DeCaria et al. (2005) of midlatitude storms in rural northeast Colorado. The removal of 15% in Bucsela et al. (2019) is based on the <20% background found in the cases by DeCaria. Using this approach, referred to as Method-15, 15% of the OMI LNO_x^* column was removed, with the remainder assumed to be fresh lightning-produced NO_x. An alternate method used was to subtract an aircraft-based boundary layer contribution from the OMI LNO_x^* column. In this method, boundary layer contributions were calculated for each 1-km layer and summed from the top of the cloud to the OMI optical centroid pressure (OCP). This summed amount represents all background NO_x contributing to the OMI LNO_x^* column and is then subtracted from the OMI column amounts. Removal of calculated boundary-layer contributions is called Method-BL and is described in detail in Section 3.2. Comparison of both methods is discussed further in each case study.

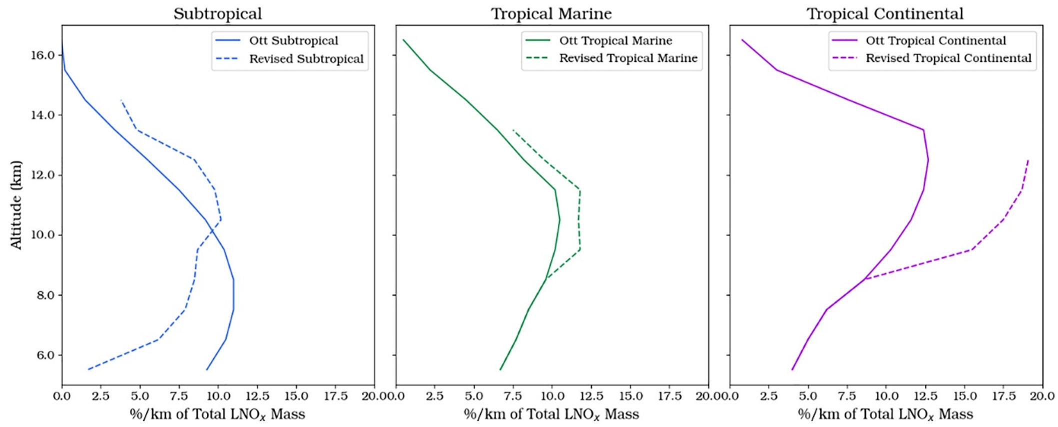

Figure 1. Original Ott et al. (2010) profiles (solid lines) of LNO_x mass percentage per km and revised amounts (dashed lines) to represent the subtropical (left), tropical marine (center), and tropical continental (right) regimes.

OMI values obtained through the approach described above in accordance with Bucsela et al. (2019) will be compared directly to aircraft column amounts to investigate the ability of the OMI satellite to retrieve columns of LNO_x.

3.2. Aircraft Analysis

Aircraft columns were obtained by summing anvil mean in-cloud values of NO and NO_2 for 1-km layers sampled by the plane at altitudes of 5–14 km. In one case, NO_x was directly provided in the archived data. Location and extent of the anvil, and all in-cloud measurements, were identified using measurements from cloud particle instrumentation and aircraft video. Refer to Table 1 for the exact method for each case. When measurements were unavailable due to instrument malfunction or no in-cloud measurements at a given altitude, missing partial column amounts were estimated in a manner that ensured that the profile shape was consistent with the most applicable LNO_x mass profile from Ott et al. (2010) (Figure 1). Ott et al. profiles have a higher vertical extent than the cases used in this study. Therefore, the LNO_x mass percent values remaining in the layers that are higher than the respective case studies of cloud top are summed and redistributed proportionally by mass into the anvil of the cloud. Further details on case-specific LNO_x mass profiles are described in Section 4. The BL contribution to the anvil measurements needs to be removed to ensure the NO_x being considered is solely produced from lightning. To achieve this via Method-15, 15% was removed from each layer before summing to find the column. To achieve this via Method-BL, it is assumed that the ratio of CO to NO_x in the boundary layer is conserved in the absence of LNO_x as a parcel is lifted in an updraft from the PBL to the anvil. This conservation is attributable to rapid transport, negligible ambient mixing or entrainment, and minimal chemical loss of NO_x and CO. It is assumed that the boundary layer air that we considered is lifted through the updraft into the anvil and does not flow around the storm and does rise above the LCL. Thus, any deviations in the total CO/NO_x ratio with height within the anvil are due to LNO_x and this fact can be exploited to extract the LNO_x signal from the measured anvil NO_x. With these assumptions, the LNO_x is given through Equation 2. Anvil and boundary layer measurements of CO are also needed as this is used as the boundary layer tracer. Following Huntrieser et al. (2008), the BL contribution was taken out of the anvil aircraft measurements by the following method:

$$LNO_x = Anvil_{NOx} - (BL_{NOx}/BL_{CO})\,Anvil_{CO} \qquad (2)$$

$Anvil_{CO}$ and BL_{CO} are measured directly by aircraft. The $BL_{NOxContribution}$, the term subtracted in Equation 2, is found for each 1 km layer. The resultant, after removing the layer-specific boundary layer NO_x contribution, is NO_x sourced only by lightning, that is, LNO_x. Anvil NO_x profiles were obtained from the partial column layers using the in situ measurements and extrapolation as discussed above. For some layers, the boundary layer contribution was larger than the measured NO_x. This caused some layers to have a negative value when BL contribution was removed using Method-BL. In these cases, the negative values are not included when obtaining the column sum as this result indicates that the plane was not measuring the direct outflow of the storm and the NO_x that is measured is either entrained or advected up from the boundary layer. See specific case studies for more information. To stay consistent with the OMI methodology, both Method-BL and Method-15 were used with the aircraft data to obtain LNO_x columns.

3.3. LNO_x Production Analysis

To determine the number of flashes contributing to the OMI and aircraft measurements of NO_x, raw flash counts are first adjusted to account for the DE of the observing system. Then, the number of contributing flashes (F) is calculated using the approach given in D. J. Allen et al. (2021) to account for NO_x lifetime (Equation 3).

$$F = \sum_{N} F_i \exp\left(-\frac{t_s - t_i}{\tau}\right) \tag{3}$$

N is the raw number of flashes detected by the lightning measuring system within the time and region of interest. Raw flashes are adjusted to account for DE. The adjusted flash value is given as F_i. The lifetime of NO_x in the near field of convection is given as τ with the flash age being given by the difference in time between flash initiation (t_i) and the time of the OMI overpass or aircraft measurement (t_s). Each storm had unique areas of consideration depending on the storm geometry and signal detected by OMI. Flashes contributing to the OMI or aircraft measurements are counted within the 6 hours preceding the final observation. Flashes were counted for a six-hour period before the overpass because uncertainties in the direction that LNO_x is transported increase greatly for longer periods making it difficult to determine if older flashes contribute to the observed column. The chemical lifetime varies with the case study and is not the determining factor when choosing the period over which flashes are summed. Extending the time window beyond 6 hours, however, would require the assumption that lightning-produced NO_x remains entirely confined within the storm during advection, an assumption that would have a strong positive bias on flash counts. The total number of moles produced from the storm derived from the OMI LNO_x columns is then divided by the number of contributing flashes to obtain the PE in moles of NO_x per flash.

An additional analysis was completed using aircraft data to determine the lifetime to use for middle and UT NO_x in the near field of convection. A previous study by B. A. Nault et al. (2016) determined a suitable range for NO_x lifetime to be 2–12 hr. This lifetime range is dependent on the ability for available NO_x to convert into methyl peroxy nitrate (MPN) or alkyl nitrates (AN). The rate of these reactions depends on the boundary layer VOC concentrations and the amount of each compound that is convectively lifted into the anvil. Measured concentrations of alkanes in the anvil were analyzed and compared to amounts found in the analysis completed by B. Nault et al. (2017) for the 21 June 2012, DC3 case. Alkanes measured included Butane-i, Butane-n, Pentane-i, Pentane-n, Cyclopentane, Hexane-n, and Heptane-n. These species were chosen as they are readily involved in the conversion of NO_x to MPNs or ANs through their ability to be oxidized by OH. According to B. A. Nault et al. (2016), the conversion into MPN or AN accounts for 70% of UT loss for NO_x. The analysis done on the 21 June case study led Nault to estimate a lifetime of 3 hr, and given the state of the boundary layer gas concentrations and the assumption, they are conserved through the updraft of the storm into the anvil. The lifetime of NO_x for each case is scaled based on this analysis and will be described further in each case. Further insights on the lifetime of NO_x and the laboratory findings can be found in B. A. Nault et al. (2016).

4. Case Study Analyses

Although there were many cases within these chosen field campaigns, very few met the requirements for this analysis. It was necessary to have the storm sampled within a short time period of the OMI instrument overpass. Furthermore, even if the aircraft and OMI measurements were taken within a reasonable time period of each other, it was necessary for the OMI data to contain a significant NO_x signature. These two requirements made the number of viable cases very small. The three cases that were chosen fit both criteria.

4.1. 11 June 2012

A midlatitude mesoscale convective system initiated from a line of storms in northwest Iowa at 2300 UTC on 10 June and became well organized in north-central Iowa at 0500 UTC on 11 June. The MCS traversed toward the southeast across Missouri and Illinois (Figure 2). This storm was observed during the Deep Convective Clouds and Chemistry (DC3) campaign (Barth et al., 2015) and was sampled by the NASA DC-8, NSF/NCAR GV, and DLR Falcon aircraft, which all left Salina, KS at ∼1600 UTC on 11 June. The Falcon made multiple in-cloud

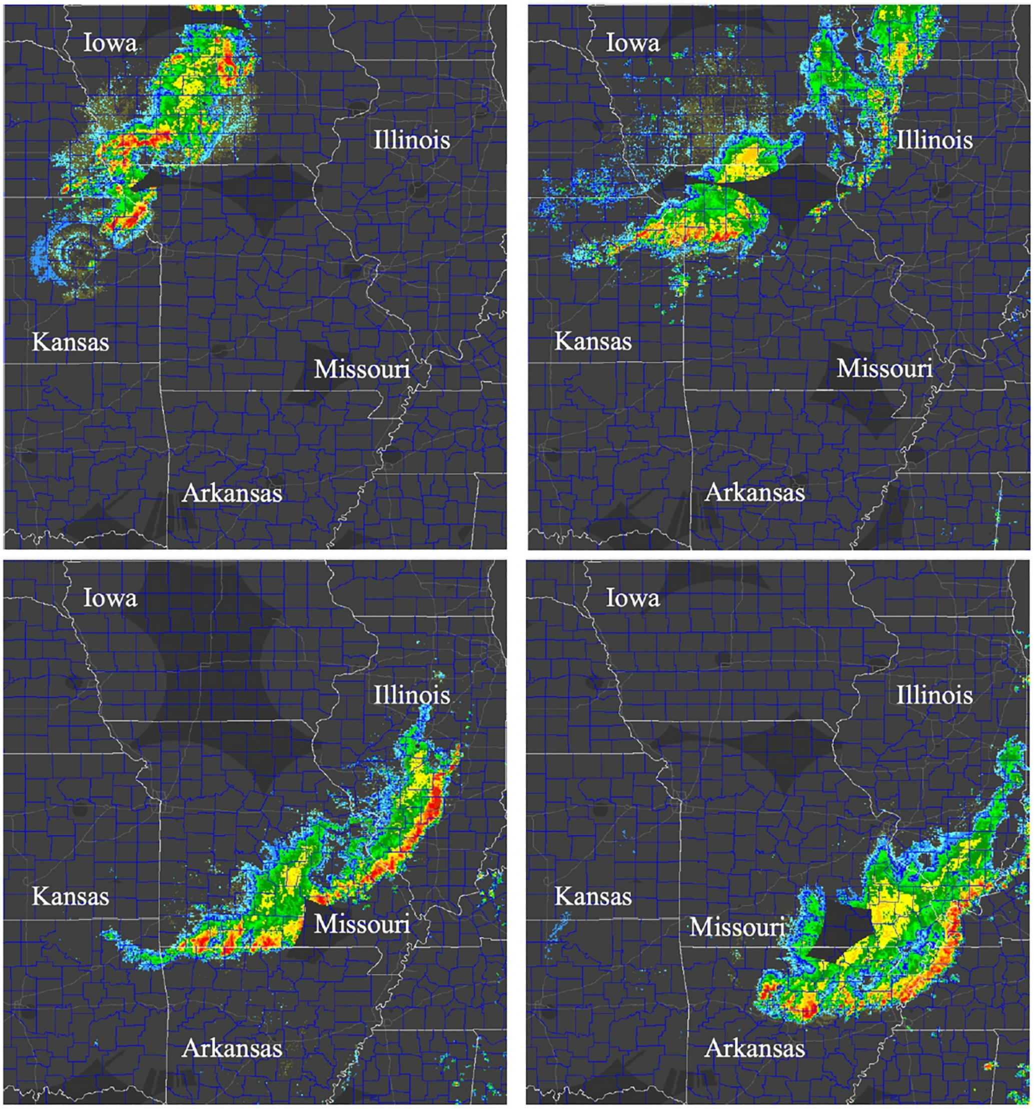

Figure 2. Composite reflectivity 11 June 2012. Top left—05:00 UTC, top right—10:00 UTC, bottom left—17:00 UTC, bottom right—20:00 UTC. Convection in southwestern and central Iowa at 05:00 UTC and traversing to Central Missouri by 15:00 UTC. The last reflectivity plot shows the MCS entering northeastern Arkansas and extending up through Southern Illinois.

transects through the rear anvil of the storm near the main cells, while the GV and DC-8 stayed in the anvil but near the outflow. The GV sampled the rear outflow, while the DC-8 measured the leading edge of the storm system and also sampled the boundary layer inflow in rural northern Alabama ahead of the system. While the GV and DC-8 sampled the MCS outflow and inflow, respectively, later in the day, these later measurements were not used in this analysis as they occurred more than 2 1/2 hr after the OMI overhead pass. Further details on the MCS are given in Li et al. (2017). Sampling periods for each aircraft, in UTC, are as follows: GV, 16:35–17:10; DC-8, 17:20–17:58; and Falcon, 17:20–18:25. Sampling period of OMI was 19:38–19:50 UTC.

4.1.1. OMI Analysis

In the 11 June 2012 OMI LNO_x retrieval, it is assumed that the vertical distribution of LNO_x mass per kilometer matches that of the subtropical profile given by Ott et al. (2010). The large OMI signature associated with this MCS had a spatial extent of 34–41°N and 92.5–87°W (Figure 3). Due to the OMI row anomaly, values west of

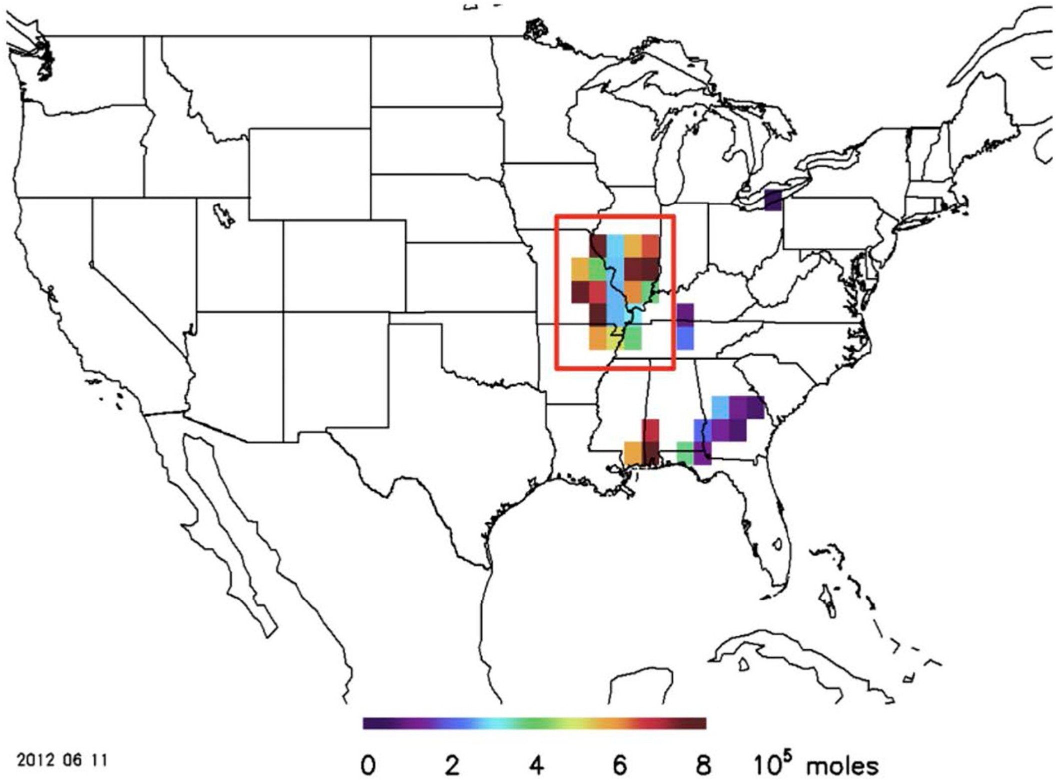

Figure 3. 1° × 1° gridded ozone monitoring instrument LNO_x^* signature for 11 June 2012. Column amounts in units of 10^5 mol. Amounts shown are before background subtractions. Signature used for analysis shown in red box, over eastern Missouri, central and southern Illinois with slight signature in Arkansas and Tennessee.

92.5°W are not available. Before background contributions were subtracted, OMI retrieved an average column amount of 3.44×10^{15} molecules/cm^2. Applying the two methods to account for boundary layer contributions, the adjusted OMI LNO_x total column amounts averaged 2.93×10^{15} molecules/cm^2 with a standard deviation of 1.21×10^{15} molecules/cm^2 following Method-15 and 1.95×10^{15} molecules/cm^2 with a standard deviation of 1.43×10^{15} molecules/cm^2 following Method-BL.

4.1.2. Aircraft Analysis

For each aircraft analysis, measurements being considered for the production of LNO_x were those that were taken inside the anvil of the storm. Determination of an "in-cloud" measurement was different for each aircraft. The DC-8 plane had a forward-facing video camera onboard. Analysis of the video provided a Cloud-Indicator Variable (CIV) that can be found in the data archive. The CIV had the classifications of 0—no cloud, 1—light cloud, 2—cloud, and 3—heavy cloud. Measurements that were taken aboard the plane that corresponded to a CIV of 1 or above were used for LNO_x evaluation. In-cloud measurements for the GV corresponded to when the particle concentration measured by the NCAR 2D-S probe was above 1 L^{-1}. The Falcon determined in-cloud measurements using the forward scattering spectrometer probe. Measurements corresponding to values equal to or above 1 cm^{-3} were deemed in-cloud. The DC-8 made a pass through the westernmost portion of the storm and around to the forward anvil of the storm from 17:20 to 17:58 UTC. During this pass, the DC-8 flew at altitudes of 7–12 km. The GV made anvil passes behind the storm from 16:35to 17:10 UTC taking measurements for altitudes 9–14 km. The Falcon made several passes on the western edge of the storm sampling from 17:20 to 18:35 UTC. Measurements from the Falcon aircraft were taken at altitudes 9–12 km. Boundary layer sampling was completed only by the DC-8 from 18:50 to 20:10 UTC in a region well ahead of the storm system. Tropopause analysis from Li et al. (2017) has the top of the cloud reaching 15 km. The Ott subtropical profile used in filling unmeasured layers reached 17 km. Ott et al. (2010) recommends that the subtropical profile be used in the northern hemisphere May-September as far as 40°N. Deep convection in the Central United States mainly

10.1029/2024JD043253

develops in subtropical air masses. Airflow into this storm came from the south/southeast. While this storm only reached 15 km, the maximum LNO_x from the aircraft observations were found between 10 and 12 km, rather than the 6–10 km in the Ott profile. Therefore, mass percent values for the Ott subtropical profile were shifted up to 2 km from the 6–7 km layer and above to account for a difference in which layers would have the most LNO_x. Shifting of the mass percent values up to 2 km was done by taking the percent value for the layer, multiplying the value by the pressure difference from the top to the bottom of the desired layer and then dividing by the original layer's change in pressure (Equation 4).

$$\text{New\%Value} = (\text{LNO}_x\text{Mass\%Value}_{L0}) * ((\Delta\ P_{L1})/(\Delta\ P_{L0})) \quad (4)$$

Applying Equation 4 to the Ott subtropical profile allows for a more accurate representation of the storm system being analyzed while conserving the shape of the profile. The remaining LNO_x mass percent in layers 13–17 km was redistributed into the anvil levels of the cloud, 10–15 km.

For 11 June, BL measurements were taken during a low-level flight segment made by the DC-8 in northern Alabama ahead of the storm of interest. Because the GV and Falcon did not complete low-level passes, the measurements taken by the DC-8 were used to calculate BL contributions for the other two aircraft. Missing CO values were filled in via linear interpolation for the 7–8 km layer. A missing layer at 12–13 km was filled in to be consistent with Li et al. (2017) who found that the 11–12 km layer value is equal to the 12–13 km layer. The top layer of 14–15 km was not measured by any plane. CO values in this layer were set to stratospheric levels, that is, the average of values at times when corresponding measurements of ozone exceeded 100 ppbv. The value for the 13–14 km layer was obtained by interpolating between the assumed values for 11–12 and 14–15 km.

Ideally, profiles should be calculated using measurements from the region sampled by OMI. However, due to the OMI row anomaly, some of the flight paths of the DC-8 and GV and most of the flight path of the Falcon were outside the valid measurement area of the satellite. To increase the representativeness of the aircraft measurements of the area sampled by OMI, a scaling factor was applied to the in situ data. Mean in-cloud aircraft NO_x amounts from the DC-8 and GV were found as a function of height for the entire flight and also for the region sampled by OMI. Unfortunately, the aircraft only sampled the OMI region when it was at altitudes of 11–12 km. Therefore a scaling factor, the ratio of the 11–12 km mixing ratio over the OMI sampling area to the 11–12 km mixing ratio for the entire in-cloud flight, was obtained and applied by multiplication to the values for each of the other layers of all in-cloud data. For instance, the mean NO_x mixing ratio between 11 and 12 km within the OMI sampling region is 0.921 ppbv compared to 0.792 ppbv for the same altitude range across the entire in-cloud flight. The ratio of these values (0.921/0.792 = 1.16) serves as the aircraft-based scaling factor for this case. The resulting weighted profile was consistent with the 11–12 km sampling in the OMI region and was then compared with what the OMI measured. The scaling factor for the DC-8 was 1.16 and for the GV it was 0.61. The entire area sampled by the Falcon was west of the OMI sampling region, and so there were no values available to create a direct ratio from Falcon measurements. Because of this, the value for the 11–12 km layer in the OMI sampled area from the DC-8 was used, and a scaling ratio of 0.55 was obtained. The DC-8 value was used because its samples were taken in closer proximity to the Falcon than the GV samples.

Figure 4 shows the partial column values for each aircraft before and after background removal with layers directly measured by the aircraft denoted by a star. In the partial column profiles, of note is the GV 13–14 km layer. Values in this layer are very large, a factor of 4 larger than in the 12–13 km layer. However, this layer had less than half as many valid measurements as the other GV measured layers likely because the aircraft did not sample above 13.1 km. Therefore, the value used for the entire layer is only a characteristic of the very bottom portion of the layer. Thus, the GV values for the 13–14 km layer may not be representative of the entire 13–14 km layer and could cause a high bias in the total GV column. Total column values were calculated from the top of the cloud (15 km, i.e. tropopause) to the optical centroid pressure (OCP) measured by the OMI. The average OCP from the OMI was 390 hPa which translates to 7 km ± 1 km. This was done for all three planes and the resulting column amounts following Method-15 were 1.82×10^{15} (DC-8), 6.53×10^{15} (GV), and 5.74×10^{15} (Falcon) molecules/cm^2. Following Method-BL, column amounts were 1.24×10^{15} (DC-8), 6.29×10^{15} (GV), and 5.46×10^{15} (Falcon) molecules/cm^2. It should be noted that the partial column amounts for the DC-8 showed negative values between 7 and 10 km. These layers are not representative of the storm outflow. An analysis of the wind profile was completed for this plane (Figure 5), and at altitudes of 7–9 km, the plane is experiencing

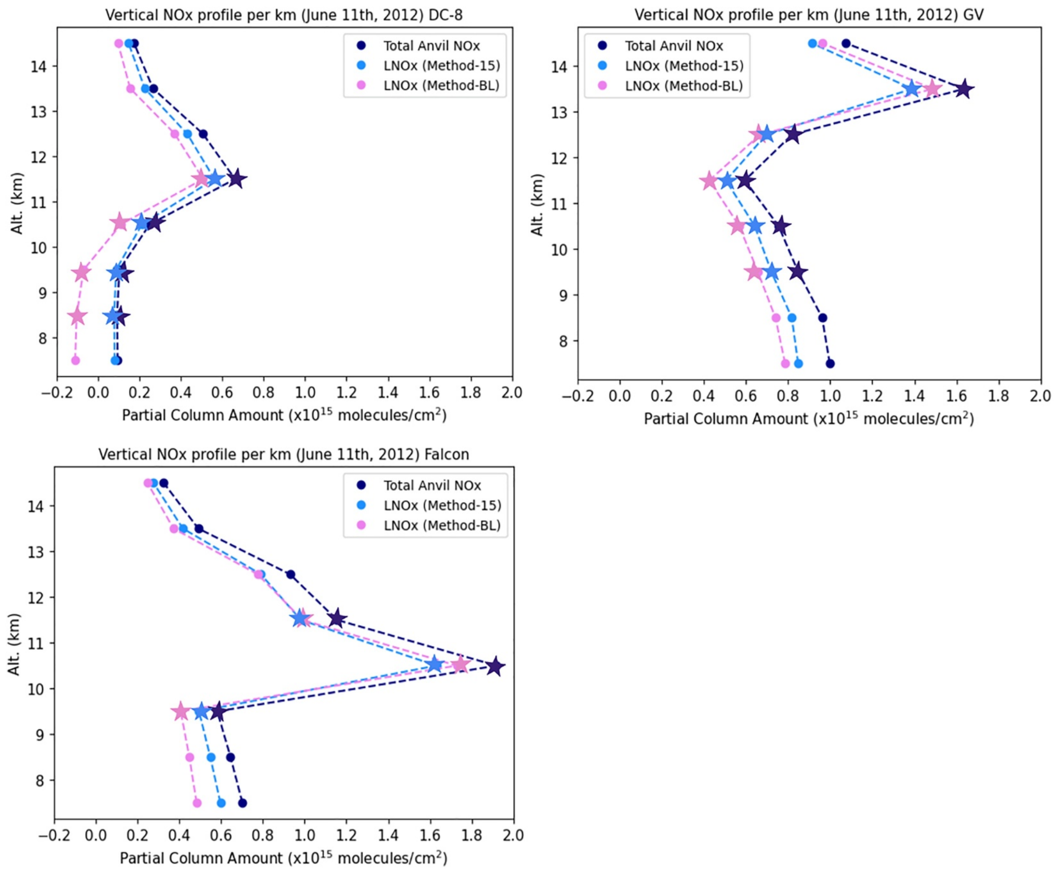

Figure 4. 11 June vertical profile of LNO_x partial column amounts for DC-8 (top left), GV (top right), and Falcon (bottom left). Stars denote layers that were measured by aircraft, and circles denote layers filled according to Ott et al. (2010) updated profiles.

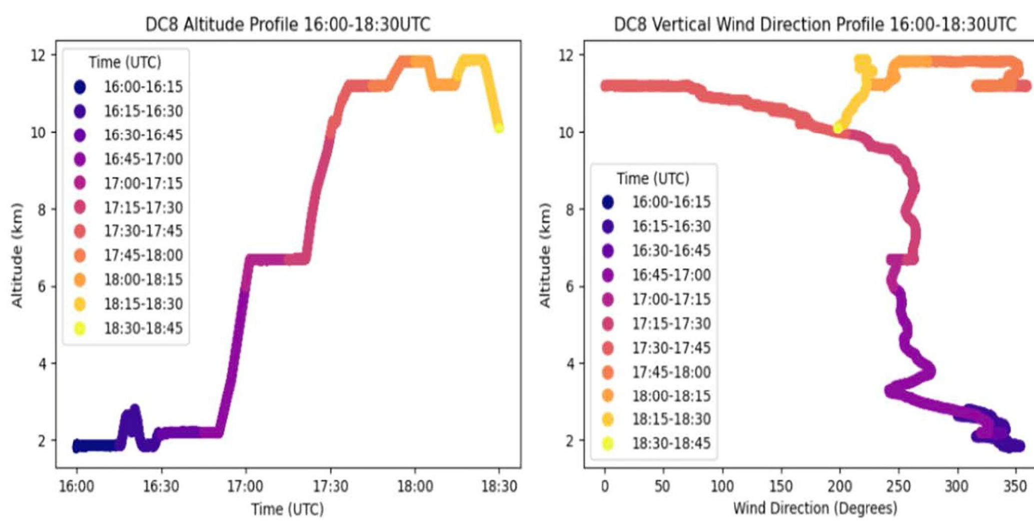

Figure 5. DC-8 vertical wind profile for 11 June. Color scale depicts time of measurement for both altitude and wind directions. Used in justification for not using negative values in the aircraft column.

10.1029/2024JD043253

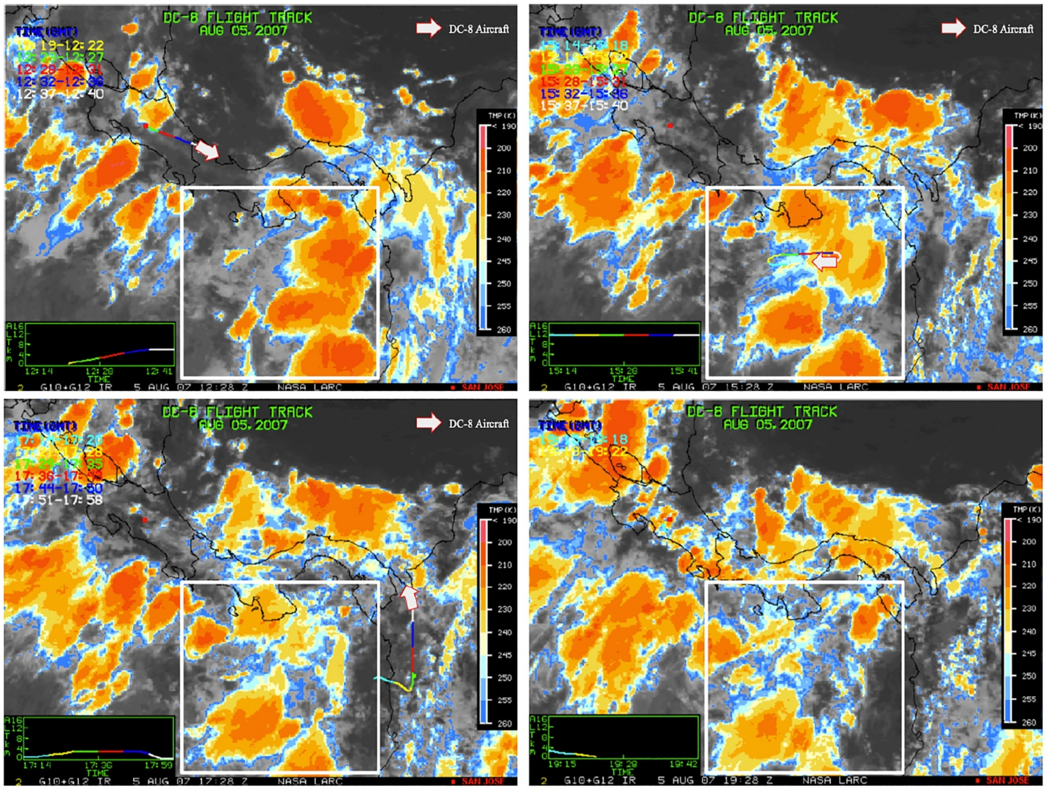

Figure 6. DC-8 flight tracks superimposed on GOES infrared brightness temperature images (Toon et al., 2010). 5 August 2007 top left—12:28 UTC, top right—15:28 UTC, bottom left—17:28 UTC, bottom right—19:28 UTC. Plane leaving San José, Costa Rica in the first image and sampling the convective system in the Gulf of Panama in the 15:28 UTC imagery. Boundary layer sampling was completed over the open ocean before the plane tracks through western Colombia and back to Costa Rica in the last image shown. White box shows the area of considered ozone monitoring instrument measurements.

dominant flow from the west/southwest. This flow is from outside of the storm, whereas fresh anvil flow is from the north with respect to the location of the plane. For this reason, these layers are not included in the analysis.

Overall, while these values differ greatly between aircraft, it is not surprising as these planes sampled different parts of the storm. In this study, we assume that the mean of these three values is a good representation of the average LNO_x produced in this case. Mean values of 4.69×10^{15} molecules/cm^2 for Method-15 and 4.32×10^{15} molecules/cm^2 for Method-BL were found through this analysis. Comparison to the OMI column amounts (2.93 and 1.95×10^{15}), for the respective methods, shows the mean OMI column is 38% and 55% smaller than the mean aircraft column.

The OMI to the aircraft difference for Method-15 is slightly larger than the uncertainty range of ±36% given by Bucsela et al. (2019), described in Section 5. The LNO_x column determined using Method-BL is outside the range obtained by Bucsela et al. (2019). A portion of these errors could result from the 13–14 km GV aircraft partial column not being representative of the entire layer.

4.2. 5 August 2007

As a part of the TC^4 campaign (Toon et al., 2010), one convective system was sampled out of the many present over south Central America, northeast Colombia, and adjacent oceans on 5 August 2007. Convection initiated in the early morning hours off the west coast of Colombia and moved westward. Most sampling of convection occurred over the Gulf of Panama, where the DC-8, WB57, and the ER-2 were present (Figure 6). For this system, NO_x was only measured by the DC-8. Anvil passes were made both over land and over water. Boundary layer sampling occurred over the ocean off the western coast of Colombia to measure storm in-flow. Periods of in-cloud

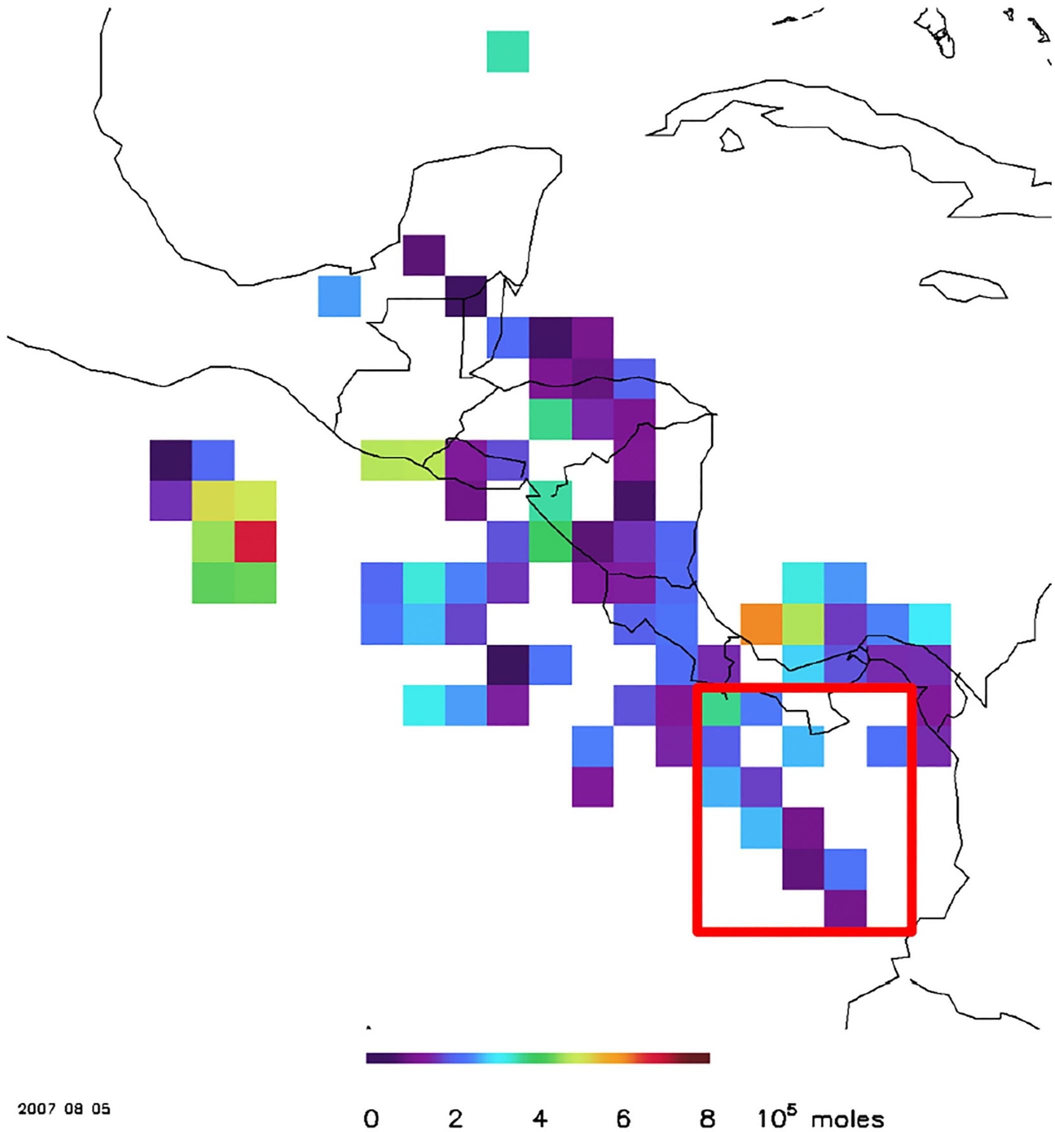

Figure 7. 1° × 1° gridded ozone monitoring instrument LNO_x^* signature for 5 August 2007. Column amounts in units of 10^5 mol. Amounts shown are before background subtraction. Pixels within the red box are used for analysis. All pixels considered are over the Gulf of Panama.

sampling by the DC-8 were 12:30-19:15 UTC and the OMI overpass time used for analysis was 19:48–20:05 UTC.

4.2.1. OMI Analysis

The OMI signature on the 5th of August extended from 5 to 10°N and 84 to 77°W and was not as uniform as for the 11 June case. Grid cells were chosen based on their relative location to the storm cells measured by the DC-8 and the pixels analyzed in Bucsela et al. (2010). The OMI LNO_x^* signature plot is shown in Figure 7. The average column amount of raw OMI LNO_x^* is 1.05×10^{15} molecules/cm^2, where this amount was obtained with an AMF whose shape function was obtained from the tropical marine profile of Ott et al. (2010). The Method-15 column amount came to be 0.89×10^{15} molecules/cm^2. Removing the aircraft-derived boundary layer contribution (Method-BL), the average OMI column becomes 0.59×10^{15} molecules/cm^2.

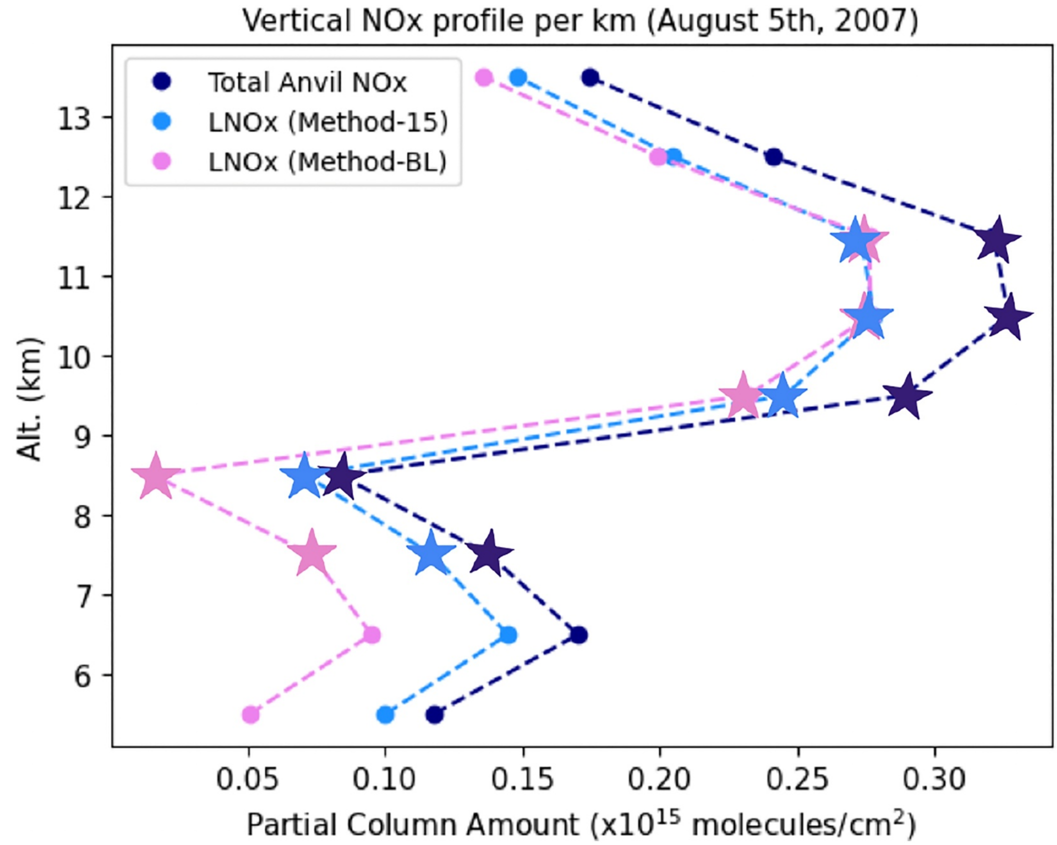

Figure 8. Partial column amounts of LNO_x for 5 August 2007. Vertical scale from top of cloud to optical centroid pressure. Stars denote layers that were measured by aircraft, and circles denote layers filled according to Ott et al. (2010) updated profiles.

4.2.2. Aircraft Analysis

The DC-8 left San José, Costa Rica at 12:22 UTC and quickly ascended to an altitude of 8 km and above by 13:00 UTC. From here, the plane made multiple anvil transects through the western portion of a storm in the Gulf of Panama. Just after 16:00 UTC, the plane began its descent in the eastern basin of the Gulf of Panama and completed a thorough boundary layer sampling. One more upper-level anvil pass was made behind the storm of interest around 18:30 UTC; however, the storm was already decaying at this time. The plane landed at around 19:30.

A vertical profile of NO_x was constructed from the aircraft measurements by computing the mean NO and NO_2 per km and adding them together. Values for layers with no valid aircraft measurements were chosen to be consistent with the Ott et al. (2010) tropical marine profile, which in this case was adjusted to account for the IR-brightness temperature-based cloud-top height of 14 km (Toon et al., 2010). Consequently, the LNO_x mass percentages from the layers 14–17 km in the Ott et al. (2010) profile were distributed to the 9–14 km layers as described previously in Section 3.2 (see Figure 1). These layers are representative of the anvil of the cloud. Boundary layer contributions of NO_x for the 5 August storm were less than that of the 11 June case as the inflow of the storm was located over a clean marine area. Sampling off the coast of Colombia provided mean boundary layer mixing ratios of 113 ppbv for CO and 0.067 ppbv of NO_x. BL NO_x contributions computed in Equation 2 were then subtracted from the in-cloud measurements from the aircraft data resulting in partial column amounts of LNO_x per km, Method-BL. A full profile of partial columns of NO_x per km from the cloud top to the OCP of 5 km for this storm can be seen in Figure 8. Before the boundary layer contribution was removed from the profile, the average column amount was 1.86×10^{15} molecules/cm^2. Although boundary layer pollution was considered negligible by Bucsela et al. (2010) due to the fact the storm was over open water, for consistency with the other two case studies, both the Method-15 and Method-BL approaches were used to determine the background

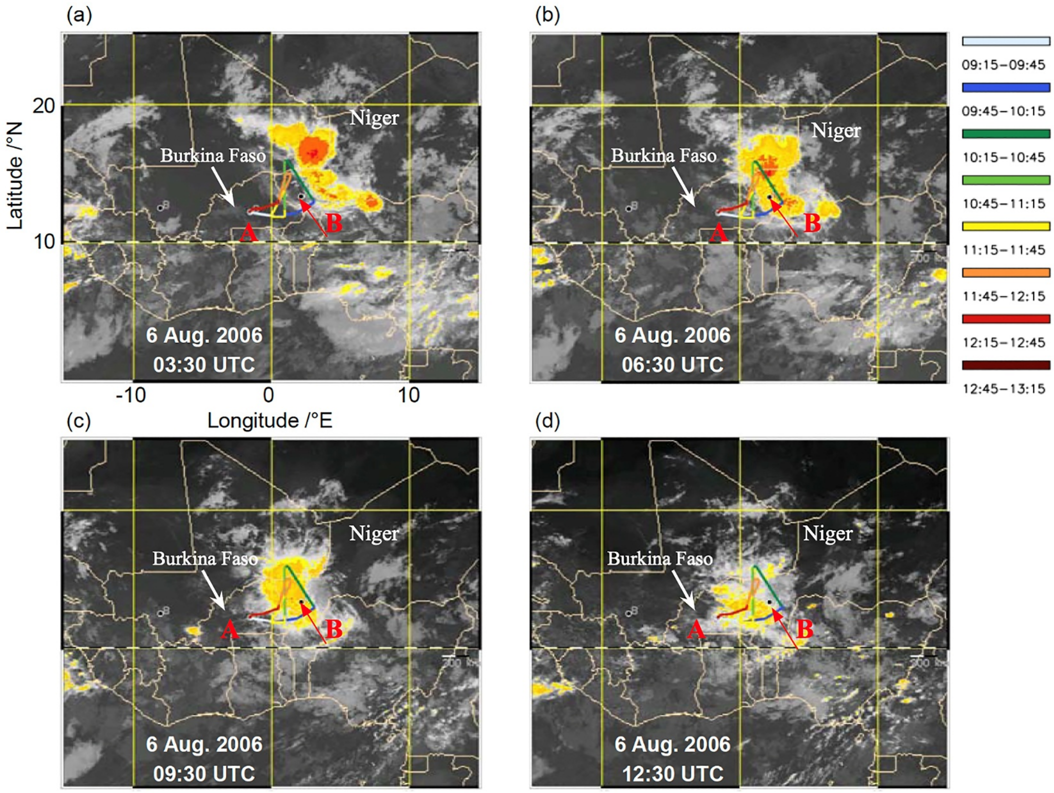

Figure 9. Falcon flight track superimposed on Meteostat Second Generation brightness temperature (Huntrieser et al., 2011) for 6 August 2006. (a) 03:30 UTC, (b) 06:30 UTC, (c) 09:30, and (d) 12:30 UTC. Flight track shows the aircraft leaving Ougadougou, Burkina Faso (red A) and sampling near Niamey, Niger (red B).

contribution. Removing the boundary layer via Method-BL resulted in a mean total column amount of 1.35×10^{15} molecules/cm^2, while Method-15 yielded 1.58×10^{15} molecules/cm^2.

Comparing OMI column amounts to the aircraft column amounts, the OMI column following Method-BL is 56% smaller than the aircraft derived column. The Method-15 column amount came to be 0.89×10^{15} molecules/cm^2, making the OMI column using Method-15 44% smaller than the aircraft column following Method-15. Once again, the difference between these values and the OMI value is a bit larger than the 36% uncertainty given in Bucsela et al. (2019).

4.3. 6 August 2006

A well-developed MCS passed over easternmost Mali and Niamey, Niger early on 6 August and proceeded southwest where it reached Ouagadougou, Burkina Faso by 12:00 UTC. The MCS was observed by the DLR-Falcon aircraft during the African Monsoon Multidisciplinary Analyses (AMMA) campaign beginning at 09:23 UTC when the storm was beginning to decay. Flight path and brightness temperature satellite imagery can be seen in Figure 9. Much of the flight occurred above 8 km where multiple anvil passes were made. A boundary layer sampling period was not explicitly designated in the flight plan, but some measurements in the upper BL were made while the plane was in descent to Ouagadougou. The Falcon sampled between 09:34 and 12:34 UTC, while the OMI overpass occurred between 13:48 and 14:24 UTC.

4.3.1. OMI Analysis

The OMI satellite measured a small signal over Western Africa associated with the storm of interest. Bounds of consideration are 10–15°N and 2°W–8°E (Figure 10). The average column amount was 0.92×10^{15} molecules/cm^2 before the removal of the boundary layer contribution. After the removal of the BL contribution, the average

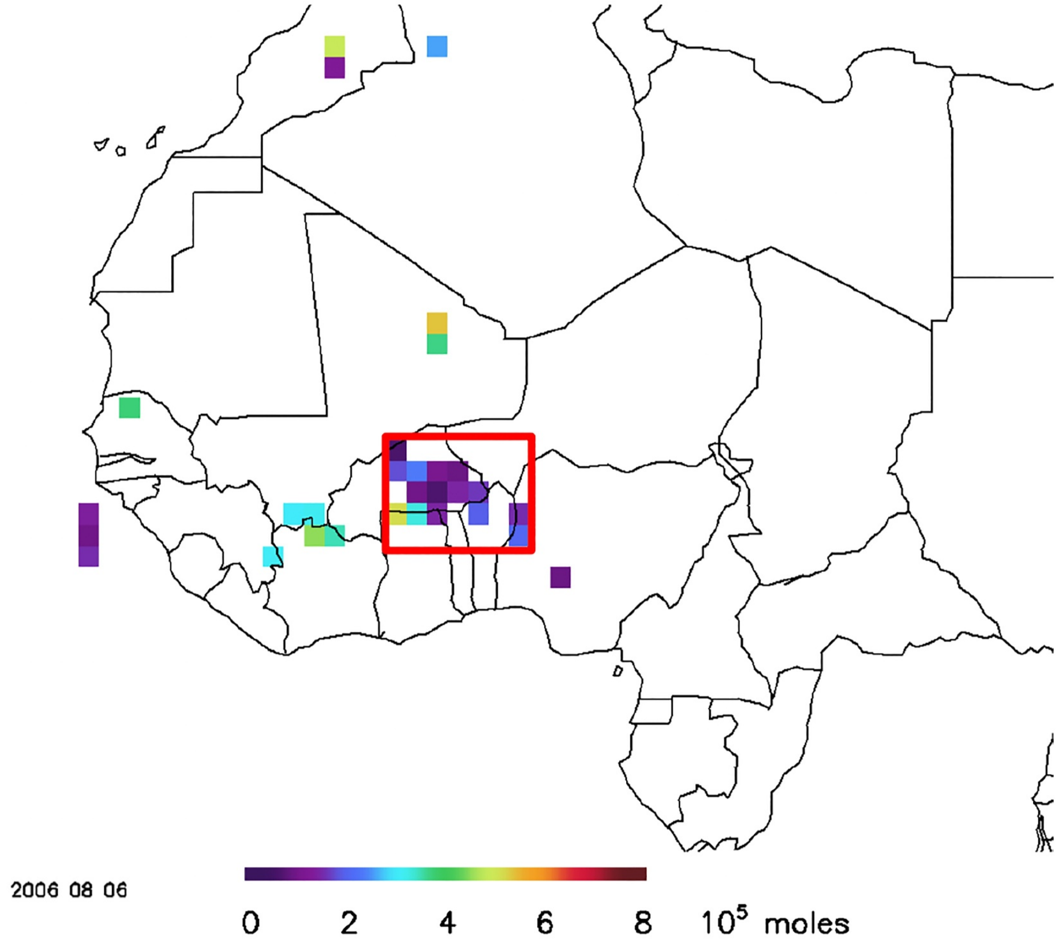

Figure 10. 1° × 1° gridded ozone monitoring instrument (OMI) $LNO_x{}^*$ signature for 6 August 2007. Column amounts in units of 10^5 mol. Amounts shown are before background subtractions. Pixels within the red box are used for analysis. OMI signature spans Burkina Faso and northern edges of Ghana, Togo, and Benin. Two pixels are in the western most portion of Nigeria.

column amount of LNO_x equaled 0.78×10^{15} molecules/cm^2 for Method-15 and 0.35×10^{15} molecules/cm^2 for Method-BL.

4.3.2. Aircraft Analysis

The aircraft measurements and observations during the 6 August case were analyzed in the study by Huntrieser et al. (2011). NO_2 was not measured by the Falcon but was calculated via the photostationary steady state assumption using measurements of NO, O_3, $J(NO_2)$, pressure, and temperature. From 9:34 to 12:00 UTC, the aircraft made anvil passes through the already decaying MCS. The measured cloud-top height reached 13 km on this day according to brightness temperature plots in Huntrieser et al. (2011), with an OCP of 7 km. Similar to the previous two analyses, estimates of values for the layers that were not measured by the aircraft were made according to a case-specific profile (see Figure 1) based on Ott et al. (2010). The location of this storm justifies the use of the tropical continental profile. For the case specific profile, the remaining layers from 13 km and above are redistributed into the anvil of the cloud, 9–13 km.

To determine the BL contribution to the UT composition, the boundary layer measurements reported by Huntrieser et al. (2011) are used along with the average CO and NO_x concentrations measured in the brief descent period of the Falcon aircraft. Boundary layer CO measurements averaged 120 ppbv and boundary layer NO_x was 0.16 ppbv. These two values are characteristic of the upper boundary layer. The use of these boundary layer aircraft measurements to represent inflow air, however, is problematic for this case. Boundary sampling occurred

10.1029/2024JD043253

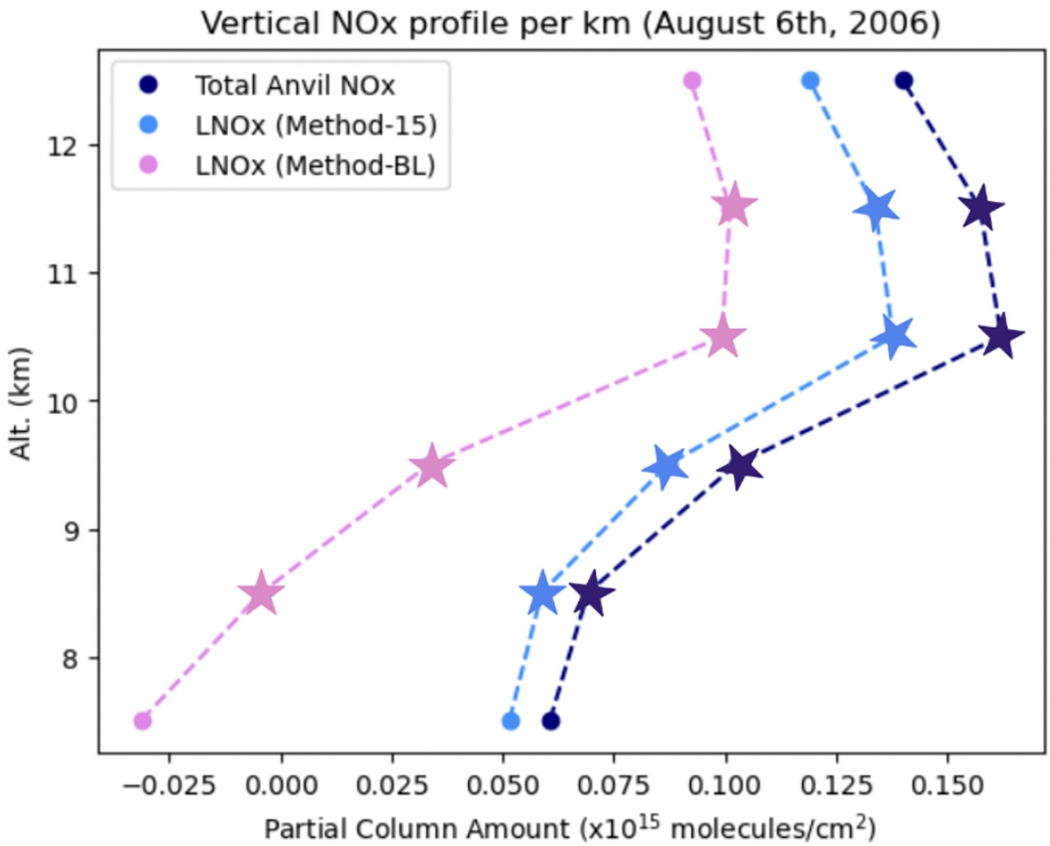

Figure 11. Partial column amounts of LNO_x for 6 August 2006. Vertical scale from top of cloud to optical centroid pressure. Stars denote layers that were measured by aircraft, and circles denote layers filled according to Ott et al. (2010) updated profiles.

during the descent period from 12:25 to landing at 12:34 UTC. When the plane entered the boundary layer, it was within a 60-km range of Ouagadougou, Burkina Faso, a large city with a significant source of anthropogenic NO_x. In addition, inflow into a large portion of this storm was not from urban areas. To make the aircraft measured boundary layer a more accurate representation of what was being ingested into the storm, the monthly (August 2006) OMI NO_2 Level 3 averages over the flight region were compared over rural and urban locations. Urban NO_2 averages were a factor of 1.5 greater than that over rural areas. Therefore, the boundary layer contribution from the aircraft was adjusted downward by a factor of 1.5 to represent inflow-air from the more rural area that covered the majority of the area of convection in Figure 9. The resulting vertical distribution of partial column amounts of LNO_x can be seen in Figure 11. Before boundary layer NO_x was removed, average column amounts were 0.69×10^{15} molecules/cm^2. It was mentioned in Huntrieser et al. (2011) that most of the NO_x measured by the aircraft was due to boundary layer contributions. Following Method-15, the LNO_x column amount for this case was 0.59×10^{15} molecules/cm^2. After the removal of boundary layer contributions for Method-BL, the remaining LNO_x column equaled 0.29×10^{15} molecules/cm^2, which agrees with the Huntrieser et al. (2011) assertion. When subtracting the aircraft-based boundary layer NO_x contribution, there was one layer with a negative value. This value was not considered representative of outflow and was not used in determining the total column amounts. Compared to the OMI column amount, the OMI column is higher than the aircraft by ~32% and ~21%, respectively.

5. LNO_x Production Efficiency Analysis

5.1. 11 June 2012

The lightning data used in the 11 June 2012 storm are that of ENTLN. As with the OMI columns, flashes must be summed over the entire system not just the region sampled by OMI. This is especially important here

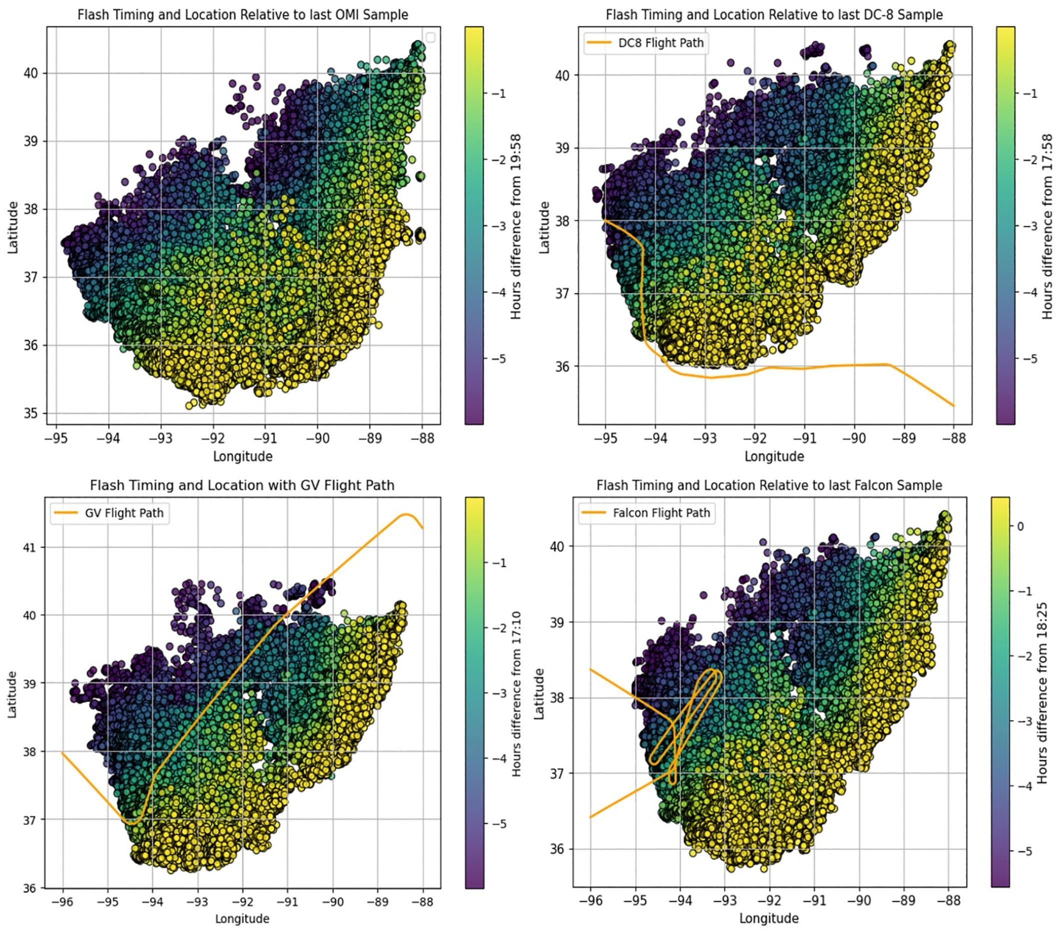

Figure 12. Flight tracks with flash location timing respective of last measurement made by ozone monitoring instrument (top left), GV (top right), DC-8 (bottom left), Falcon (bottom right) 11 June 2012.

because wind measurements from the GV show flow from the southwest indicating that flashes southwest of the plane's motion affected the LNO_x total. From the GV plot in Figure 12, it can be seen that the GV sampled an area that had witnessed the effect of lightning for a long time with the majority of the storm passing over the sampled area. Wind profiles of the GV aircraft can be found in Figure S1 in Supporting Information S1. This is in contrast to the DC-8 that had measured winds from the north and mostly sampled freshly produced LNO_x off the leading edge anvil of the storm. The same reasoning for the inclusion of the use of the entire storm area for flash count is used for the Falcon. Measured winds from the Falcon were predominantly from the south and southwest with advection from this region contributing to the LNO_x totals. Wind profiles for the Falcon can be found in Figure S2 in Supporting Information S1. Wind profiles for all three aircraft were analyzed at the time of their sampling. The wind direction at the time of sampling for the GV and Falcon shows flow coming in from the west. To account for NO_x advection, flashes west of the aircraft flight leg are included. Therefore, bounds of flash consideration for all planes and OMI spanned from 88 to 95.5° West and 35–42° degrees North. As indicated by the GV and Falcon winds, there is advection of LNO_x eastward from the lightning in the western portion of the storm. For this reason, flashes from the entire storm are also counted when determining flashes affecting OMI. For the OMI, flash consideration began at 13:58 UTC and continued to 19:58, which marked the last measured LNO_x signal from OMI for this storm. The raw ENTLN measured flashes were 110,627. Accounting for DE, total flashes equaled 165,286. After applying Equation 3 to account for LNO_x lifetime, total flashes affecting the OMI measurements were 116,544. After a comparison of anvil VOC measurements of this case and that of 21 June 2012 from B. Nault et al. (2017), the VOC concentrations of this case study were roughly half of those observed on 21 June. For this reason, a lifetime of 6 hr is being used here rather than the 3 hr obtained by Nault for 21 June. Uncertainty in our comparison of OMI- and aircraft-based

Table 2
Ozone Monitoring Instrument Total Signature Amounts in Mmoles for Each Case Study

Case	OMI LNO_x^* (Mmoles)	OMI LNO_x Method-15 (Mmoles)	OMI LNO_x Method-BL (Mmoles)
11 June	10.89	9.36	6.14
5 August	2.55	2.17	1.38
6 August	2.77	2.35	1.12

LNO_x column amounts and PE also arises because lightning occurred at times between the end of aircraft sampling and the OMI overpass time. The same analysis was completed for the number of flashes contributing to the aircraft measurements. Flashes were totaled from the 6 hr prior to the last in-cloud sample completed by the aircraft. Time bounds are as follows (11:10–17:10, GV), (11:58–17:58, DC-8), and (12:25–18:35, Falcon). Following the same method as used for OMI, flash statistics can be seen in Table 3. Comparing to the OMI total of 116,544 flashes, flash totals at the times of the aircraft measurements were 26.6%, 24.8%, and 23.8% less than the totals at the time of the OMI overpass for the GV, DC-8, and Falcon, respectively.

Dividing the moles of OMI LNO_x (Table 2) by the total flash counts (Table 3) yields estimates of PE. The total OMI signature of LNO_x equaled 9.26 Mmoles following Method-15 and 6.14 Mmoles following Method-BL. For this storm, 80 mol/flash were obtained following Method-15 and 52 mol/flash were obtained following Method-BL. The PE values found in this case are slightly lower than PE estimates made by previous case study analyses of DC3 storms. I. Pollack et al. (2016) found a range of 101–533 mol/flash for seven volume-based case analyses in the DC3 campaign through ground-based Lightning Mapping Array lightning data and airborne NO_x observations. Pickering et al. (2024) obtained a low PE range of 80–110 mol/flash for a high flash rate DC3 storm. A sensitivity analysis was conducted for the 11 June case to assess the uncertainty associated with the assumed NO_x lifetime. Adjusting the NO_x lifetime to 9 hr resulted in a 10% decrease in PE, while extending the lifetime to 12 hr led to a 15% decrease in PE. Accordingly, the uncertainty in PE for this case study is estimated to be the upper value of 15%. The range of PE values for all three cases is shown in Table 4.

5.2. 5 August 2007

Flash counts for the 5 August case study were obtained from WWLLN stroke data for the 6 hr (14:05–20:05 UTC) prior to the OMI overpass over the region (5–10°N) and (84–77°W). The area of consideration for OMI grid cells was chosen to stay consistent with Bucsela et al. (2010). WWLLN strokes require a DE correction and a means of translation to flashes. As described in Bucsela et al. (2010), the corrections were obtained by comparing the total number of WWLLN strokes with flash counts from the Costa Rica Lightning Detection Network (CRLDN) after those counts were corrected for DE using the Lightning Imaging Sensor (LIS). The raw WWLLN stroke counts were increased by a factor of 4.57 to match the DE corrected CRLDN flash counts. Thus, the 876 detected strokes for contributing to the OMI measurements were assumed to represent 4,003 flashes. We assumed a NO_x lifetime of 12 hr for the 5 August as VOCs were negligible in the boundary layer sampling done over the ocean. This is the upper bound of lifetime provided by B. Nault et al. (2017). After applying Equation 3 and adjusting for DE, 3,141 flashes were found to contribute to the OMI satellite LNO_x^* column. The last aircraft measurement was 19:15 UTC, so flash consideration begins at 13:15 UTC for the DC-8. Raw flash totals from WWLLN are 952. After accounting for DE, total flashes were 4,350, and accounting for lifetime, the final count was 3,462.

Accounting for the two methods in which OMI LNO_x columns were found, the PE is 691 mol/flash for Method-15 and 439 mol/flash for Method-BL. It is unsurprising that the PE for this low flash rate marine convection case was larger than that for the high flash rate land-based 11 June case. This contrast also aligns well with the findings of Huntrieser et al. (2008), who found that greater LNO_x production occurs in storms with stronger vertical wind shear. Bucsela et al. (2010) reported that anvil-level winds for the 5 August case ranged from 8 to 13 m/s, placing it on the stronger side compared to the other three cases analyzed in the TC^4 campaign. From the analysis by Bucsela et al. (2010), the PE was determined to be 227 ± 223 mol/flash after removing the background tropospheric NO_2 contribution using the GMI model. The PE

Table 3
Total Flashes Affecting Ozone Monitoring Instrument and Aircraft Measurements for 11 June 2012

	OMI	GV	DC-8	Falcon
Raw ENTLN	110,637	89,445	91,360	92,009
After D.E. Correction	165,286	132,637	135,729	136,771
Final Total	116,544	85,548	87,629	88,711

Note. Final totals represent raw flash counts adjusted using Equation 3.

Table 4
Production Efficiency Range Based on Ozone Monitoring Instrument Measurements for Each Case Study

Case	PE range (moles/flash)
11 June 2012	52–80
5 August 2007	439–691
6 August 2006	205–431

values obtained for this study, following our new method, are higher than the mean given Bucsela et al. (2010). The differences in PE values arise because in the 2010 study, the lifetime of NO_x was not accounted for. Clearly, the long duration of this convective system adds uncertainty to the PE estimate.

5.3. 6 August 2006

The 6 August case used lightning data from the DLR Lightning Location Network (LINET) (Höller et al., 2009) and WWLLN. Unfortunately, the LINET sensors were not functional until 11:03 UTC on the day of the storm. In light of this, WWLLN data will be used for this case and will be scaled to LIS flashes according to D. J. Allen et al. (2019). To stay consistent with the other analyses, strokes contributing to the OMI column will be summed from 6 hr prior to the last OMI measurement which was at 14:21 UTC. By the time the aircraft began measuring, the MCS was in a decaying stage. Stroke rates were low, but rather constant. WWLLN data from 08:24 to 14:24 UTC measured 290 strokes. A comparison between the number of WWLLN strokes and LINET strokes was made for the time period where both data sets were available. From 11:03 to 14:21 UTC, there were 52 WWLLN strokes and 1,962 LINET strokes. This provides a 2.6% DE for WWLLN relative to LINET. This DE for this case matches well with the DE of WWLLN with respect to LIS flashes for this region given in D. J. Allen et al., 2019. For this reason, WWLLN data will be used for the entire time period and scaled following the 2.6% DE to convert to LIS-equivalent flashes. This results in a total of 11,165 flashes. Like the previous analyses, the flashes then need to be adjusted according to Equation 3 to determine the number of flashes contributing to the OMI LNO_x. A lifetime of 6 hr is being used for this case. This lifetime is based on comparison to those used for the other two cases and also looking at the monthly average of OMI HCHO for August 2006 in Western Africa, as a proxy for VOCs. There were no VOC measurements from the Falcon for this case. However, there was confirmed heightened amounts of CO and NO_x from the aircraft in the upper troposphere due to urban influence. Therefore, a lifetime of 6 hr (similar to the 11 June case) would serve this case well. When accounting for lifetime using Equation 3, total contributing flashes equaled 5,446 for OMI. The flashes contributing to the aircraft were measured from 06:34 to 12:34 UTC. Raw flashes measured 662 and accounting for DE and lifetime resulted in a total of 12,862 flashes. The total OMI LNO_x following Method-15 for this case was 2.35 Mmoles and following Method-BL was 1.12 Mmoles. The resulting PE estimates for OMI were 431 mol/flash and 205 mol/flash, respectively. In an analysis of the 6 August storm based on the aircraft observation of NO_x, Huntrieser et al. (2011) found a PE of about 179 mol of NO_x per flash. Our findings are larger than those from the 2011 study.

6. Discussion

The differences between aircraft-derived column amounts and OMI column amounts in the 11 June and 5 August cases were larger than for the 6 August case (Table 5). The OMI LNO_x column was 38%–56% smaller than the aircraft column amount in those two cases, despite the fact that the number of flashes contributing to the OMI values were on average, 25% greater than for the aircraft. Another area of uncertainty lies in the missing OMI values due to the OMI row anomaly in the 11 June case. While this was able to be mended for the PE calculation in the 11 June case, missing pixels could have contributed to the much lower OMI column amounts. Overall, 11 June was a very high flash rate storm and the low production efficiencies align well with the understanding that LNO_x production per flash is inversely related to flash rate (Bucsela et al., 2019).

Table 5
LNO_x Total Column Amounts for Method-15 and Method-BL in Molecules/cm^2

	Method-15 Aircraft	Method-BL Aircraft	Method-15 OMI	Method-BL OMI	Percent difference Method-15 (%)	Percent difference Method-BL (%)
11 June	4.69×10^{15}	4.32×10^{15}	2.93×10^{15}	1.95×10^{15}	−38	−55
5 August	1.58×10^{15}	1.35×10^{15}	0.89×10^{15}	0.59×10^{15}	−44	−56
6 August	0.59×10^{15}	0.29×10^{15}	0.78×10^{15}	0.35×10^{15}	+32	+21

Note. Column amounts listed for 11 June are averaged across the three planes. Percent differences show the difference in column amounts between the two methods shown for the aircraft and ozone monitoring instrument (OMI). Positive (negative) percent difference indicates the OMI column was larger (smaller).

The 5 August OMI overpass experienced roughly 300 less flashes than the aircraft and the column amount was 46%–56% smaller than that from the aircraft. Production efficiency amounts ranging from 439 to 691 mol/flash are on the higher side, but reasonable as production efficiencies are believed to be larger over the ocean where flash energies are larger and flashes are fewer (D. J. Allen et al., 2019; Beirle et al., 2014). The 6 August case had the lowest percent difference between the OMI and aircraft column. For Method-15 and Method-BL, differences were 32% and 21%, respectively, with OMI having larger column values than the aircraft. In this case, the aircraft was exposed to more than double the flashes as OMI because the storm was already in a decaying stage when OMI sampled, resulting in a decay of the LNO_x signal. In the previous two cases, the OMI significantly underestimated the mean column LNO_x produced, but was exposed to nearly the same number of flashes (5 August) or 25% more (11 June) than the aircraft. 6 August was the only case where aircraft was exposed to more than the OMI and the only case where the OMI column amount was larger than the aircraft. The 6 August case had a lower PE than the 5 August despite them both being in the tropics. This result is in agreement with D. J. Allen et al. (2019) that concluded that LNO_x PE is approximately two times larger over marine locations than over continental locations in the tropics. Production efficiencies for the 6 August are 205 and 431 mol/flash, which is within the range given by literature over a tropical continental region.

In the Bucsela et al. (2019) study, the uncertainty range of ±36% for LNO_x columns is derived from multiple sources of potential errors. Briefly put here, sources of errors include smoothing of stratospheric contributions to mitigate the unintended assigning of tropospheric signals to the stratosphere. This smoothing would affect the OMI retrieved column total in a positive bias. Furthermore, uncertainties in OMI LNO_x retrieved values arise from errors in background estimates (lofted pollution, advection) and LNO_x lifetime. Uncertainty also stems from the assumed NO_2 profiles and AMF calculated by the OMI retrievals. The Bucsela et al. (2019) AMF was computed with the GMI NO_2 and NO_x profiles and provides the largest source of error in PE values. In the current study, the AMF is computed using profiles from Ott et al. (2010), but uncertainty likely remains similar. Accounting for all potential uncertainties gives a total of ±36% error in OMI retrieved values. For the six estimates of percentage difference between aircraft and OMI LNO_x columns, three are larger than 36%, two are approximately equivalent, and one is smaller (Table 5).

7. Conclusion

LNO_x columns derived using NO_x profiles obtained via aircraft observations from three field campaigns were compared to OMI-based columns that were determined following the methods of Bucsela et al. (2019). For the 11 June and 5 August cases, a ∼50% percent difference was found between OMI and aircraft columns. This difference is a bit larger than the uncertainty range given by Bucsela et al. (2019). For a large flash density storm, like 11 June, the OMI-based method underestimated the LNO_x columns when compared to the aircraft column. The OMI LNO_x column was also smaller than the aircraft-profile-based column over the ocean for the TC^4 case. The 6 August case column amounts for the two observation platforms were 20%–30% different from one another. The better agreement between OMI and aircraft-based LNO_x columns for the AMMA 6 August case could be fortuitous given the concerns about contamination from the PBL, but it is encouraging. Overall, the results from the three case studies provide support for the continued use of OMI data, as well as that from newer satellite instruments such as TROPOMI and TEMPO, in examining LNO_x columns over storms. The mean difference between OMI and aircraft columns of 41% is near the uncertainty range (36%) suggested by Bucsela. The large variability in results between the individual case studies illustrates the uncertainties in the aircraft-based and satellite-based approaches and emphasizes the need for additional case studies using aircraft sampling with complete in-cloud profiles of storms with low-and-high flash densities.

The production efficiencies found for these three case studies range from 52 to 691 mol/flash. Factors contributing to the large range of values for individual case studies include uncertainties associated with the handling of boundary layer contributions, missing layers, the retrieved LNO_x^* values, and the lifetime adjustment needed to determine the number of contributing flashes. The sensitivity of the lifetime to anvil VOC concentrations adds additional uncertainty, but if VOC observations are available, a more accurate PE can be obtained.

The results of this study highlight the critical importance of conducting additional aircraft measurement campaigns to capture more detailed vertical profiles of LNO_x production from thunderstorms. These efforts are essential for improving our understanding of lightning-induced NO_x distributions throughout the atmosphere.

Data Availability Statement

Aircraft data for the DC3 campaign can be found in data archives at https://www-air.larc.nasa.gov/cgi-bin/ArcView/dc3. Similarly, for the TC4 campaign, aircraft data can be found at https://espoarchive.nasa.gov/archive/browse/tc4/DC8. Data from AMMA needed for this study can be found through the HALO database, https://doi.org/10.17616/R39Q0T. Specific data set numbers are as follows: Meteorology: #10750 Release #1, NO and NO_y: #10762 Release #1, NO_x: #10774 Release #1, CO: #10796 Release #1, FSSP: #10808 Release #1. AMMA Campaign URL: https://halo-db.pa.op.dlr.de/mission/57. For more information on data used, refer to Huntrieser et al. (2011). WWLLN data are available through the University of Washington, while ENTLN measurements can be obtained by contacting the Earth Networks support team located at https://ghrc.nsstc.nasa.gov/home/content/earth-networks-total-lightning-network-entln-global-lightning-network. OMI LNO_x^* data sets used to generate plots and figures can be accessed through Seiler and Bucsela (2024) from the Digital Repository at the University of Maryland (DRUM). The research products archived in DRUM will be available indefinitely. The University of Maryland Libraries' DRUM repository is built on DSpace software, a widely used, reliable digital repository platform. DRUM performs nightly bit-level integrity tests on all files, and all contents are regularly copied to back-up storage. DRUM conforms to the digital preservation principles outlined in the University of Maryland Libraries' Digital Preservation Policy.

Acknowledgments
ENTLN lightning: Jeff Lapierre at Earth Networks. WWLLN: Robert Holzworth at the University of Washington. Trace gas observations and cloud measurements: Andy Weinheimer, Ilana Pollack, Tom Ryerson, Glenn Diskin, Donald Blake, Paul Lawson, Teresa Campos, Ron Cohen, Hans Schlager. Funding: NASA ACCDAM Grant 80NSSC21K1345. Further DLR data availability: Michael Lichtenstern, Paul Stock, Anke Roiger, Monika Scheibe, Andreas Minikin. Use of Bucsela et al. (2010) Figure 2. License Number: 5921421127762.

References

Allen, D., Pickering, K., Duncan, B., & Damon, M. (2010). Impact of lightning NO emissions on North American photochemistry as determined using the Global Modeling Initiative (GMI) model. *Journal of Geophysical Research*, *115*(D22), D22301. https://doi.org/10.1029/2010jd014062

Allen, D., Pickering, K., Pinder, R., Henderson, B., Appel, K., & Prados, A. (2012). Impact of lightning-NO on eastern United States photochemistry during the summer of 2006 as determined using the CMAQ model. *Atmospheric Chemistry and Physics*, *12*(4), 1737–1758. https://doi.org/10.5194/acp-12-1737-2012

Allen, D. J., Pickering, K. E., Bucsela, E., Krotkov, N., & Holzworth, R. (2019). Lightning NO_x production in the tropics as determined using OMI NO_2 retrievals and WWLLN stroke data. *Journal of Geophysical Research: Atmospheres*, *124*(23), 13498–13518. https://doi.org/10.1029/2018jd029824

Allen, D. J., Pickering, K. E., Lamsal, L., Mach, D. M., Quick, M. G., Lapierre, J., et al. (2021). Observations of lightning NO_x production from GOES-R post launch test field campaign flights. *Journal of Geophysical Research: Atmospheres*, *126*(8), e2020JD033769. https://doi.org/10.1029/2020jd033769

Barth, M. C., Cantrell, C. A., Brune, W. H., Rutledge, S. A., Crawford, J. H., Huntrieser, H., et al. (2015). The deep convective clouds and chemistry (DC3) field campaign. *Bulletin of the American Meteorological Society*, *96*(8), 1281–1309. https://doi.org/10.1175/bams-d-13-00290.1

Beirle, S., Huntrieser, H., & Wagner, T. (2010). Direct satellite observation of lightning-produced NO_x. *Atmospheric Chemistry and Physics*, *10*(22), 10965–10986. https://doi.org/10.5194/acp-10-10965-2010

Beirle, S., Koshak, W., Blakeslee, R., & Wagner, T. (2014). Global patterns of lightning properties derived by OTD and LIS. *Natural Hazards and Earth System Sciences*, *14*(10), 2715–2726. https://doi.org/10.5194/nhess-14-2715-2014

Beirle, S., Spichtinger, N., Stohl, A., Cummins, K., Turner, T., Boccippio, D., et al. (2006). Estimating the NO_x produced by lightning from GOME and NLDN data: A case study in the Gulf of Mexico. *Atmospheric Chemistry and Physics*, *6*(4), 1075–1089. https://doi.org/10.5194/acp-6-1075-2006

Bucsela, E. J., Pickering, K. E., Allen, D. J., Holzworth, R. H., & Krotkov, N. A. (2019). Midlatitude lightning NO_x production efficiency inferred from OMI and WWLLN data. *Journal of Geophysical Research: Atmospheres*, *124*(23), 13475–13497. https://doi.org/10.1029/2019jd030561

Bucsela, E. J., Pickering, K. E., Huntemann, T. L., Cohen, R. C., Perring, A., Gleason, J. F., et al. (2010). Lightning-generated NO_x seen by the ozone monitoring instrument during NASA's tropical composition, cloud and climate coupling experiment (TC4). *Journal of Geophysical Research*, *115*, D10. https://doi.org/10.1029/2009jd013118

Cummings, K. A., & Cummings, K. (2013). Lightning flash rate and chemistry simulation of tropical island convection using a cloud-resolved model. *Chemical Physics*, *13*, 2757–2777.

DeCaria, A. J., Pickering, K. E., Stenchikov, G. L., & Ott, L. E. (2005). Lightning-generated NO_x and its impact on tropospheric ozone production: A three-dimensional modeling study of a stratosphere-troposphere experiment: Radiation, aerosols and ozone (STERAO-) thunderstorm. *Journal of Geophysical Research*, *110*(D14), 1–13. https://doi.org/10.1029/2004jd005556

DeCaria, A. J., Pickering, K. E., Stenchikov, G. L., Scala, J. R., Stith, J. L., Dye, J. E., et al. (2000). A cloud-scale model study of lightning-generated NO_x in an individual thunderstorm during STERAO-A. *Journal of Geophysical Research*, *105*(D9), 11601–11616. https://doi.org/10.1029/2000jd900033

Dowden, R. L., Brundell, J. B., & Rodger, C. J. (2002). VLF lightning location by time of group arrival (TOGA) at multiple sites. *Journal of Atmospheric and Solar-Terrestrial Physics*, *64*(7), 817–830. https://doi.org/10.1016/s1364-6826(02)00085-8

Finney, D., Doherty, R., Wild, O., Huntrieser, H., Pumphrey, H., & Blyth, A. (2014). Using cloud ice flux to parametrise large-scale lightning. *Atmospheric Chemistry and Physics*, *14*(23), 12665–12682. https://doi.org/10.5194/acp-14-12665-2014

Finney, D. L., Doherty, R. M., Wild, O., Stevenson, D. S., MacKenzie, I. A., & Blyth, A. M. (2018). A projected decrease in lightning under climate change. *Nature Climate Change*, *8*(3), 210–213. https://doi.org/10.1038/s41558-018-0072-6

Gerbig, C., Kley, D., Volz-Thomas, A., Kent, J., Dewey, K., & McKenna, D. S. (1996). Fast response resonance fluorescence CO measurements aboard the C-130: Instrument characterization and measurements made during North Atlantic regional experiment 1993. *Journal of Geophysical Research*, *101*(D22), 29229–29238. https://doi.org/10.1029/95jd03272

Gerbig, C., Schmitgen, S., Kley, D., Volz-Thomas, A., Dewey, K., & Haaks, D. (1999). An improved fast-response vacuum-UV resonance fluorescence CO instrument. *Journal of Geophysical Research*, *104*(D1), 1699–1704. https://doi.org/10.1029/1998jd100031

Höller, H., Betz, H.-D., Schmidt, K., Calheiros, R., May, P., Houngninou, E., & Scialom, G. (2009). Lightning characteristics observed by a VLF/LF lightning detection network (LINET) in Brazil, Australia, Africa and Germany. *Atmospheric Chemistry and Physics*, *9*(20), 7795–7824. https://doi.org/10.5194/acp-9-7795-2009

Huntrieser, H., Schlager, H., Lichtenstern, M., Roiger, A., Stock, P., Minikin, A., et al. (2009). NO_x production by lightning in Hector: First airborne measurements during SCOUT-O3/ACTIVE. *Atmospheric Chemistry and Physics*, *9*(21), 8377–8412. https://doi.org/10.5194/acp-9-8377-2009

Huntrieser, H., Schlager, H., Lichtenstern, M., Stock, P., Hamburger, T., Höller, H., et al. (2011). Mesoscale convective systems observed during AMMA and their impact on the NO_x and O_3 budget over West Africa. *Atmospheric Chemistry and Physics*, *11*(6), 2503–2536. https://doi.org/10.5194/acp-11-2503-2011

Huntrieser, H., Schlager, H., Roiger, A., Lichtenstern, M., Schumann, U., Kurz, C., et al. (2007). Lightning-produced NO_x over Brazil during TROCCINOX: Airborne measurements in tropical and subtropical thunderstorms and the importance of mesoscale convective systems. *Atmospheric Chemistry and Physics*, *7*(11), 2987–3013. https://doi.org/10.5194/acp-7-2987-2007

Huntrieser, H., Schumann, U., Schlager, H., Höller, H., Giez, A., Betz, H.-D., et al. (2008). Lightning activity in Brazilian thunderstorms during TROCCINOX: Implications for NO_x production. *Atmospheric Chemistry and Physics*, *8*(4), 921–953. https://doi.org/10.5194/acp-8-921-2008

Jamali, S., Klingmyr, D., & Tagesson, T. (2020). Global-scale patterns and trends in tropospheric NO_2 concentrations, 2005–2018. *Remote Sensing*, *12*(21), 3526. https://doi.org/10.3390/rs12213526

Koshak, W., Peterson, H., Biazar, A., Khan, M., & Wang, L. (2014). The NASA lightning nitrogen oxides model (LNOM): Application to air quality modeling. *Atmospheric Research*, *135*, 363–369. https://doi.org/10.1016/j.atmosres.2012.12.015

Labrador, L. J., von Kuhlmann, R., & Lawrence, M. G. (2004). Strong sensitivity of the global mean OH concentration and the tropospheric oxidizing efficiency to the source of NO_x from lightning. *Geophysical Research Letters*, *31*(6), D14303. https://doi.org/10.1029/2003gl019229

Lamsal, L. N., Krotkov, N. A., Vasilkov, A., Marchenko, S., Qin, W., Yang, E.-S., et al. (2021). Ozone monitoring instrument (OMI) Aura nitrogen dioxide standard product version 4.0 with improved surface and cloud treatments. *Atmospheric Measurement Techniques*, *14*(1), 455–479. https://doi.org/10.5194/amt-14-455-2021

Lapierre, J. L., Laughner, J. L., Geddes, J. A., Koshak, W. J., Cohen, R. C., & Pusede, S. E. (2020). Observing US regional variability in lightning NO_2 production rates. *Journal of Geophysical Research: Atmospheres*, *125*(5), e2019JD031362. https://doi.org/10.1029/2019jd031362

Lawson, R. P., O'Connor, D., Zmarzly, P., Weaver, K., Baker, B., Mo, Q., & Jonsson, H. (2006). The 2D-s (stereo) probe: Design and preliminary tests of a new airborne, high-speed, high-resolution particle imaging probe. *Journal of Atmospheric and Oceanic Technology*, *23*(11), 1462–1477. https://doi.org/10.1175/jtech1927.1

Lay, E., Rodger, C., Holzworth, R., & Dowden, R. (2005). Introduction to the world wide lightning location network (WWLLN). In *Geophysical research abstract* (Vol. 7).

Lay, E. H., Holzworth, R. H., Rodger, C. J., Thomas, J. N., Pinto, O., Jr., & Dowden, R. L. (2004). WWLL global lightning detection system: Regional validation study in Brazil. *Geophysical Research Letters*, *31*(3), 5. https://doi.org/10.1029/2003gl018882

Levelt, P. F., Van Den Oord, G. H., Dobber, M. R., Malkki, A., Visser, H., De Vries, J., et al. (2006). The ozone monitoring instrument. *IEEE Transactions on Geoscience and Remote Sensing*, *44*(5), 1093–1101. https://doi.org/10.1109/tgrs.2006.872333

Li, Y., Pickering, K. E., Allen, D. J., Barth, M. C., Bela, M. M., Cummings, K. A., et al. (2017). Evaluation of deep convective transport in storms from different convective regimes during the DC3 field campaign using WRF-Chem with lightning data assimilation. *Journal of Geophysical Research: Atmospheres*, *122*(13), 7140–7163. https://doi.org/10.1002/2017jd026461

Liaskos, C. E., Allen, D. J., & Pickering, K. E. (2015). Sensitivity of tropical tropospheric composition to lightning NO_x production as determined by replay simulations with GEOS-5. *Journal of Geophysical Research: Atmospheres*, *120*(16), 8512–8534. https://doi.org/10.1002/2014jd022987

Liu, F., Beirle, S., Zhang, Q., Van Der A, R. J., Zheng, B., Tong, D., & He, K. (2017). NO_x emission trends over Chinese cities estimated from OMI observations during 2005 to 2015. *Atmospheric Chemistry and Physics*, *17*(15), 9261–9275. https://doi.org/10.5194/acp-17-9261-2017

Lorente, A., Folkert Boersma, K., Yu, H., Dörner, S., Hilboll, A., Richter, A., et al. (2017). Structural uncertainty in air mass factor calculation for NO_2 and HCHO satellite retrievals. *Atmospheric Measurement Techniques*, *10*(3), 759–782. https://doi.org/10.5194/amt-10-759-2017

Marais, E. A., Jacob, D. J., Choi, S., Joiner, J., Belmonte-Rivas, M., Cohen, R. C., et al. (2018). Nitrogen oxides in the global upper troposphere: Interpreting cloud-sliced NO_2 observations from the OMI satellite instrument. *Atmospheric Chemistry and Physics*, *18*(23), 17017–17027. https://doi.org/10.5194/acp-18-17017-2018

Marchand, M., Hilburn, K., & Miller, S. D. (2019). Geostationary lightning mapper and earth networks lightning detection over the contiguous United States and dependence on flash characteristics. *Journal of Geophysical Research: Atmospheres*, *124*(21), 11552–11567. https://doi.org/10.1029/2019jd031039

Marchenko, S., Krotkov, N., Lamsal, L., Celarier, E., Swartz, W., & Bucsela, E. (2015). Revising the slant column density retrieval of nitrogen dioxide observed by the ozone monitoring instrument. *Journal of Geophysical Research: Atmospheres*, *120*(11), 5670–5692. https://doi.org/10.1002/2014jd022913

Martin, R. V., Sauvage, B., Folkins, I., Sioris, C. E., Boone, C., Bernath, P., & Ziemke, J. (2007). Space-based constraints on the production of nitric oxide by lightning. *Journal of Geophysical Research*, *112*(D9), D09309. https://doi.org/10.1029/2006jd007831

Nault, B., Laughner, J., Wooldridge, P., Crounse, J., Dibb, J., Diskin, G., et al. (2017). Lightning NO_x emissions: Reconciling measured and modeled estimates with updated NO_x chemistry. *Geophysical Research Letters*, *44*(18), 9479–9488. https://doi.org/10.1002/2017gl074436

Nault, B. A., Garland, C., Wooldridge, P. J., Brune, W. H., Campuzano-Jost, P., Crounse, J. D., et al. (2016). Observational constraints on the oxidation of NO_x in the upper troposphere. *The Journal of Physical Chemistry A*, *120*(9), 1468–1478. https://doi.org/10.1021/acs.jpca.5b07824

Ott, L. E., Pickering, K. E., Stenchikov, G. L., Allen, D. J., DeCaria, A. J., Ridley, B., et al. (2010). Production of lightning NO_x and its vertical distribution calculated from three-dimensional cloud-scale chemical transport model simulations. *Journal of Geophysical Research*, *115*(D4), D04301. https://doi.org/10.1029/2009jd011880

Palmer, P. I., Jacob, D. J., Chance, K., Martin, R. V., Spurr, R. J., Kurosu, T. P., et al. (2001). Air mass factor formulation for spectroscopic measurements from satellites: Application to formaldehyde retrievals from the global ozone monitoring experiment. *Journal of Geophysical Research*, *106*(D13), 14539–14550. https://doi.org/10.1029/2000jd900772

Pérez-Invernón, F. J., Gordillo-Vázquez, F. J., van der Velde, O., Montanyá, J., López Trujillo, J. A., Pineda, N., et al. (2023). Lightning-produced nitrogen oxides per flash length obtained by using TROPOMI observations and the Ebro Lightning Mapping Array. *Geophysical Research Letters*, *50*(24), e2023GL104699. https://doi.org/10.1029/2023gl104699

Pickering, K. E., Bucsela, E., Allen, D., Ring, A., Holzworth, R., & Krotkov, N. (2016). Estimates of lightning NO_x production based on OMI NO2 observations over the Gulf of Mexico. *Journal of Geophysical Research: Atmospheres*, *121*(14), 8668–8691. https://doi.org/10.1002/2015jd024179

Pickering, K. E., Li, Y., Cummings, K. A., Barth, M. C., Allen, D. J., Bruning, E. C., & Pollack, I. B. (2024). Lightning NO_x in the 29–30 May 2012 deep convective clouds and chemistry (DC3) severe storm and its downwind chemical consequences. *Journal of Geophysical Research: Atmospheres*, *129*(11), e2023JD039439. https://doi.org/10.1029/2023jd039439

Pollack, I., Homeyer, C., Ryerson, T., Aikin, K., Peischl, J., Apel, E., et al. (2016). Airborne quantification of upper tropospheric NO_x production from lightning in deep convective storms over the United States Great Plains. *Journal of Geophysical Research: Atmospheres*, *121*(4), 2002–2028. https://doi.org/10.1002/2015jd023941

Pollack, I. B., Lerner, B. M., & Ryerson, T. B. (2010). Evaluation of ultraviolet light-emitting diodes for detection of atmospheric NO_2 by photolysis-chemiluminescence. *Journal of Atmospheric Chemistry*, *65*(2–3), 111–125. https://doi.org/10.1007/s10874-011-9184-3

Price, C., & Rind, D. (1992). A simple lightning parameterization for calculating global lightning distributions. *Journal of Geophysical Research*, *97*(D9), 9919–9933. https://doi.org/10.1029/92jd00719

Quick, M. G., Christian, H., Jr., Blakeslee, R. J., Stewart, M. F., Corredor, D., & Podgorny, S. (2017). Fly's Eye GLM simulator preliminary validation analysis. In *AGU fall meeting abstracts* (Vol. 2017).AE33A-2512.

Ridley, B., & Grahek, F. (1990). A small, low flow, high sensitivity reaction vessel for NO chemiluminescence detectors. *Journal of Atmospheric and Oceanic Technology*, *7*(2), 307–311. https://doi.org/10.1175/1520-0426(1990)007<0307:aslfhs>2.0.co;2

Rodger, C., Brundell, J., Holzworth, R., Lay, E. H., Crosby, N. B., Huang, T. Y., & Rycroft, M. J. (2009). Growing detection efficiency of the world wide lightning location network. In *AIP conference proceedings* (Vol. 1118, pp. 15–20). https://doi.org/10.1063/1.3137706

Rodger, C., Werner, S., Brundell, J. B., Lay, E. H., Thomson, N. R., Holzworth, R. H., & Dowden, R. (2006). Detection efficiency of the VLF world-wide lightning location network (WWLLN): Initial case study. *Annales Geophysicae*, *24*(12), 3197–3214. https://doi.org/10.5194/angeo-24-3197-2006

Romps, D. M., Seeley, J. T., Vollaro, D., & Molinari, J. (2014). Projected increase in lightning strikes in the United States due to global warming. *Science*, *346*(6211), 851–854. https://doi.org/10.1126/science.1259100

Ryerson, T., Williams, E., & Fehsenfeld, F. (2000). An efficient photolysis system for fast-response NO_2 measurements. *Journal of Geophysical Research*, *105*(D21), 26447–26461. https://doi.org/10.1029/2000jd900389

Sachse, G. W., Collins Jr, J. E., Hill, G., Wade, L., Burney, L. G., & Ritter, J. A. (1991). Airborne tunable diode laser sensor for high-precision concentration and flux measurements of carbon monoxide and methane. *Measurement of atmospheric gases*, *1433*, 157–166. https://doi.org/10.1117/12.46162

Schenkeveld, V., Jaross, G., Marchenko, S., Haffner, D., Kleipool, Q. L., Rozemeijer, N. C., et al. (2017). In-flight performance of the ozone monitoring instrument. *Atmospheric Measurement Techniques*, *10*(5), 1957–1986. https://doi.org/10.5194/amt-10-1957-2017

Schumann, U., & Huntrieser, H. (2007). The global lightning-induced nitrogen oxides source. *Atmospheric Chemistry and Physics*, *7*(14), 3823–3907. https://doi.org/10.5194/acp-7-3823-2007

Seiler, M., & Bucsela, E. (2024). *Vertical column densities of LNOx**. University of Maryland DRUM. https://doi.org/10.13016/wyua-muuk

Sicard, P., Agathokleous, E., De Marco, A., Paoletti, E., & Calatayud, V. (2021). Urban population exposure to air pollution in Europe over the last decades. *Environmental Sciences Europe*, *33*, 1–12. https://doi.org/10.1186/s12302-020-00450-2

Stolz, D. C., Rutledge, S. A., Pierce, J. R., & van den Heever, S. C. (2017). A global lightning parameterization based on statistical relationships among environmental factors, aerosols, and convective clouds in the TRMM climatology. *Journal of Geophysical Research: Atmospheres*, *122*(14), 7461–7492. https://doi.org/10.1002/2016jd026220

Thornton, J. A., Wooldridge, P. J., & Cohen, R. C. (2000). Atmospheric NO2: In situ laser-induced fluorescence detection at parts per trillion mixing ratios. *Analytical Chemistry*, *72*(3), 528–539. https://doi.org/10.1021/ac9908905

Toon, O. B., Starr, D. O., Jensen, E. J., Newman, P. A., Platnick, S., Schoeberl, M. R., et al. (2010). Planning, implementation, and first results of the tropical composition, cloud and climate coupling experiment (TC4). *Journal of Geophysical Research*, *115*(D10), D00J04. https://doi.org/10.1029/2009jd013073

Volz-Thomas, A., Lerner, A., Pätz, H.-W., Schultz, M., McKenna, D. S., Schmitt, R., et al. (1996). Airborne measurements of the photolysis frequency of NO_2. *Journal of Geophysical Research*, *101*(D13), 18613–18627. https://doi.org/10.1029/96jd01375

Zeldovich, Y., Frank-Kamenetskii, D., & Sadovnikov, P. (1947). *Oxidation of nitrogen in combustion*. Publishing House of the Acad of Sciences of USSR.

Zhu, Q., Laughner, J. L., & Cohen, R. C. (2019). Lightning NO_2 simulation over the contiguous US and its effects on satellite NO_2 retrievals. *Atmospheric Chemistry and Physics*, *19*(20), 13067–13078. https://doi.org/10.5194/acp-19-13067-2019

Zhu, Y., Rakov, V., Tran, M., Stock, M., Heckman, S., Liu, C., et al. (2017). Evaluation of ENTLN performance characteristics based on the ground truth natural and rocket-triggered lightning data acquired in Florida. *Journal of Geophysical Research: Atmospheres*, *122*(18), 9858–9866. https://doi.org/10.1002/2017jd027270